
Natural Resources Canada

Ressources naturelles Canada

Microstructure and Properties of Simulated Heat Affected Zones

Final Report 278-T-05 for Project

Development of Optimized Welding Solutions for X100 Line Pipe Steel

Prepared for the

Design, Materials, and Construction Technical Committee of
Pipeline Research Council International, Inc.
and
U.S. Department of Transportation
Pipeline and Hazardous Materials Safety Administration
Office of Pipeline Safety

Prepared by

J.A. Gianetto, G.R Goodall and W.R Tyson,
CANMET Materials Technology Laboratory

M.A. Quintana and V.B Rajan
The Lincoln Electric Company

Y. Chen
Center for Reliable Energy Systems

September 2011

This research was funded in part under the Department of Transportation, Pipeline and Hazardous Materials Safety Administration's Pipeline Safety Research and Development Program. The views and conclusions contained in this document are those of the authors and should not be interpreted as representing the official policies, either expressed or implied, of the Pipeline and Hazardous Materials Safety Administration, or the U.S. Government.

CANMET Materials Technology Laboratory

Microstructure and Properties of Simulated Heat Affected Zones

J.A. Gianetto, G.R Goodall, and W.R Tyson,
CANMET Materials Technology Laboratory
Minerals and Metals Sector, Natural Resources Canada
183 Longwood Road South, Hamilton, ON, Canada, L8P 0A5

M.A Quintana and V.B Rajan
Lincoln Electric Company

Y. Chen
Center for Reliable Energy Systems

CANMET Report No. 2011-06(TR)

September 2011

Catalog No. L5XXXX

Microstructure and Properties of Simulated Heat Affected Zones

Final Report 278-T-05 for Project

Development of Optimized Welding Solutions for X100 Line Pipe Steel

Prepared for the

Design, Materials, and Construction Technical Committee of
Pipeline Research Council International, Inc.
and
U.S. Department of Transportation
Pipeline and Hazardous Materials Safety Administration
Office of Pipeline Safety

Prepared by

J.A. Gianetto, G.R Goodall and W.R Tyson,
CANMET Materials Technology Laboratory

M.A. Quintana and V.B Rajan
The Lincoln Electric Company

Y. Chen
Center for Reliable Energy Systems

September 2011

Version	Date of Last Revision	Date of Uploading	Comments
2	2 April 2011	4 April 2011	References to be inserted after review.
Final	1 September 2011	1 December 2011	Final Report

This report is furnished to Pipeline Research Council International, Inc. (PRCI) under the terms of PRCI contract [278-PR- 348 - 074513], between PRCI and the MATH-1 contractors:

- Electricore (prime contractor),
- Center for Reliable Energy Systems, CANMET, NIST, and The Lincoln Electric Company (sub-contractors).

The contents of this report are published as received from the MATH-1 contractor and subcontractors. The opinions, findings, and conclusions expressed in the report are those of the authors and not necessarily those of PRCI, its member companies, or their representatives. Publication and dissemination of this report by PRCI should not be considered an endorsement by PRCI of the MATH-1 contractor and subcontractors, or the accuracy or validity of any opinions, findings, or conclusions expressed herein.

In publishing this report, PRCI and the MATH-1 contractors make no warranty or representation, expressed or implied, with respect to the accuracy, completeness, usefulness, or fitness for purpose of the information contained herein, or that the use of any information, method, process, or apparatus disclosed in this report may not infringe on privately owned rights. PRCI and the MATH-1 contractors assume no liability with respect to the use of, or for damages resulting from the use of, any information, method, process, or apparatus disclosed in this report. By accepting the report and utilizing it, you agree to waive any and all claims you may have, resulting from your voluntary use of the report, against PRCI and the MATH-1 contractors.

Pipeline Research Council International Catalog No. L5XXXX

PRCI Reports are Published by Technical Toolboxes, Inc.

3801 Kirby Drive, Suite 520
Houston, Texas 77098
Tel: 713-630-0505
Fax: 713-630-0560
Email: info@ttoolboxes.com

PROJECT PARTICIPANTS

PROJECT TEAM MEMBER	COMPANY AFFILIATION	PROJECT TEAM MEMBER	COMPANY AFFILIATION
Arti Bhatia	Alliance	Jim Costain	GE
Jennifer Klementis	Alliance	Gilmar Batista	Petrobras
Roger Haycraft	Boardwalk	Marcy Saturno de Menezez	Petrobras
David Horsley	BP	Dave Aguiar	PG&E
Mark Hudson	BP	Ken Lorang	PRCI
Ron Shockley	Chevron	Maslat Al-Waranbi	Saudi Aramco
Sam Mishael	Chevron	Paul Lee	SoCalGas
David Wilson	ConocoPhillips	Alan Lambeth	Spectra
Satish Kulkarni	El Paso	Robert Turner	Stupp
Art Meyer	Enbridge	Gilles Richard	TAMSA
Bill Forbes	Enbridge	Noe Mota Solis	TAMSA
Scott Ironside	Enbridge	Philippe Darcis	TAMSA
Sean Keane	Enbridge	Dave Taylor	TransCanada
Laurie Collins	Evraz	Joe Zhou	TransCanada
David de Miranda	Gassco	Jason Skow	TransGas
Adriaan den Herder	Gasunie	Ernesto Cisneros	Tuberia Laguna
Jeff Stetson	GE	Vivek Kashyap	Welpsun
		Chris Brown	Williams

CORE RESEARCH TEAM	
RESEARCHER	**COMPANY AFFILIATION**
Yaoshan Chen	Center for Reliable Energy Systems
Yong-Yi Wang	Center for Reliable Energy Systems
Ming Liu	Center for Reliable Energy Systems
Dave Fink	Lincoln Electric Company
Marie Quintana	Lincoln Electric Company
Vaidyanath Rajan	Lincoln Electric Company
Joe Daniel	Lincoln Electric Company
Radhika Panday	Lincoln Electric Company
James Gianetto	CANMET Materials Technology Laboratory
John Bowker	CANMET Materials Technology Laboratory
Bill Tyson	CANMET Materials Technology Laboratory
Guowu Shen	CANMET Materials Technology Laboratory
Dong Park	CANMET Materials Technology Laboratory
Timothy Weeks	National Institute of Standards and Technology
Mark Richards	National Institute of Standards and Technology
Dave McColskey	National Institute of Standards and Technology
Enrico Lucon	National Institute of Standards and Technology
John Hammond	Consultant Metallurgist & Welding Engineer

This Page Intentionally Left Blank

FINAL REPORT STRUCTURE

Focus Area 1 - Update of Weld Design, Testing, and Assessment Procedures for High Strength Pipelines		
Report #	**Description**	**Lead Authors**
277-T-01	Background of Linepipe Specifications	CRES/CANMET
277-T-02	Background of All-Weld Metal Tensile Test Protocol	CANMET/Lincoln
277-T-03	Development of Procedure for Low-Constraint Toughness Testing Using a Single-Specimen Technique	CANMET/CRES
277-T-04	Summary of Publications: Single-Edge Notched Tension SE(T) Tests	CANMET
277-T-05	Small Scale Tensile, Charpy V-Notch, and Fracture Toughness Tests	CANMET/NIST
277-T-06	Small Scale Low Constraint Fracture Toughness Test Results	CANMET/NIST
277-T-07	Small Scale Low Constraint Fracture Toughness Test Discussion and Analysis	CANMET/NIST
277-T-08	Summary of Mechanical Properties	CANMET
277-T-09	Curved Wide Plate Tests	NIST/CRES
277-T-10	Weld Strength Mismatch Requirements	CRES/CANMET
277-T-11	Curved Wide Plate Test Results and Transferability of Test Specimens	CRES/CANMET
277-S-01	Summary Report 277 Weld Design, Testing, and Assessment Procedures for High Strength Pipelines	CRES

Focus Area 2 - Development of Optimized Welding Solutions for X100 Linepipe Steel		
Report #	**Description**	**Lead Authors**
278-T-01	State of The Art Review	Lincoln
278-T-02	Material Selection, Welding and Weld Monitoring	Lincoln/CANMET
278-T-03	Microstructure and Hardness Characterization of Girth Welds	CANMET/Lincoln
278-T-04	Microstructure and Properties of Simulated Weld Metals	CANMET/Lincoln
278-T-05	Microstructure and Properties of Simulated Heat Affected Zones	CANMET/Lincoln
278-T-06	Essential Welding Variables	Lincoln/CANMET
278-T-07	Thermal Model for Welding Simulations	CRES/CANMET
278-T-08	Microstructure Model for Welding Simulations	CRES/CANMET
278-T-09	Application to Other Processes	Lincoln/CANMET
278-S-01	Summary Report 278 Development of Optimized Welding Solutions for X100 Line Pipe Steel	Lincoln

EXECUTIVE SUMMARY

This investigation is part of a major consolidated program of research that is supported by the US Department of Transportation Pipeline and Hazardous Materials Safety Administration (US DOT PHMSA) and Pipeline Research Council International (PRCI) to advance weld design, establish weld testing procedures, and assessment methodologies, and develop optimized welding solutions for joining the high strength (X100 steel pipe) being considered for frontier pipelines. Construction of long distance pipelines with high operating pressures presents several technical challenges that are addressed in this program being co-sponsored by government and industry.

Major advances in steelmaking and a move towards higher strength steel pipe to meet operational demands have come together to improve the economics of pipeline construction projects in harsh and environmentally challenging remote regions in the world. Welding is a critical step in the development of these projects and the technology to advance innovative high-productivity techniques for joining high strength steel pipe is a focal point for research. One aspect of this research is the study of weld metal (WM) and related heat-affected zone (HAZ) structure and properties. These two regions, weld metal and heat affected zone, are the subjects of this investigation and have been reported separately.

A Gleeble® thermal simulator was used to simulate HAZ microstructures and evaluate phase transformations associated with single and multipass regions of pipeline girth welds. The first step was to establish realistic thermal cycles (histories) for a wide range of welding process/procedure conditions, including GMAW-P welding. In this investigation the transformation behaviour of simulated grain coarsened heat-affected zone (GCHAZ) regions formed in three X100 pipe steels and a modern X80 pipe steel of similar composition were established by dilatometry. In addition, the notch toughness was evaluated using different simulated GCHAZ and intercritcally reheated (ICRGCHAZ) regions in order to establish the transition behaviour compared with the respective pipe steels. The initial work focused on the development of continuous cooling transformation (CCT) diagrams for the GCHAZ in three X100 pipe steels, as well as, for a modern X80 pipe steel. Differences in microstructure and hardness resulting from thermal cycles with peak temperature of 1350°C and cooling times from 800°C to 500°C ($\Delta t_{800\text{-}500}$) from 1 to 50 seconds were investigated. GCHAZ microstructures with varying proportions of lath martensite and different morphologies of bainite were found along with overall coarsening of the transformed microstructures with increasing cooing time. These changes are consistent with the corresponding reduction in hardness observed for a given pipe steel composition (hardenability). There was a trend of decreasing notch toughness for the simulated HAZ regions (reductions of absorbed energies and shift in energy transition temperature to higher temperatures) for the simulated HAZ regions compared with the respective pipe steels. The pipe steel (X100-4) with the highest hardenability resulting from additions of Ni, Cr (instead of Mo), Cu and lower Nb with optimum Ti and N exhibited the best pipe steel and HAZ toughness. This correlates with the formation of more favourable HAZ microstructures of lath martensite with fine bainite microstructures resulting from the suppression of the $\gamma \rightarrow \alpha$ transformation to lower temperatures over a wider range of cooling times.

TABLE OF CONTENTS

LIST OF FIGURES

LIST OF TABLES

1 INTRODUCTION

This investigation is part of a major consolidated program with two parallel projects that were designed with common and complementary research activities to advance the primary focus areas:

1. Update weld design, testing and assessment procedures for high strength steel pipelines [1]
2. Develop optimized welding solutions for X100 line pipe steel [2]

In the second focus area, a primary objective was to establish the key factors affecting strength and toughness of weld metal and heat affected zone regions for a range of pipeline girth welding process and procedure options. To this end, the work has been divided into two activities focused on assessment of (i) high strength steel WM, and (ii) HAZ generated in high strength steel pipes. In the first activity, selected welding consumables were used to produce welds with different chemical compositions applicable for narrow gap mechanized pipeline girth welding of high strength X100 (Grade 690) steel pipes [3]. In the second activity, which is the subject of this report, HAZ microstructure and toughness of high strength pipe steels were assessed using Gleeble®[1] thermal simulation techniques. This allowed the transformation behaviour to be characterized and microstructure and toughness correlations for thermally simulated HAZ regions to be determined. This work also helped with development and calibration of thermal-microstructure models [4, 5], and with the evaluation and interpretation of baseline pipe welds [6-11] produced and analyzed in this program.

Thermal simulation has been used to study HAZ structure and property relationships for many years with focus on a wide range of industrial applications, such as pipelines, offshore structures, and ships including the stringent requirements of submarines [10-18]. For industrial applications such as pipeline field construction, where relatively low energy inputs are used for joining pipes with narrow gap mechanized welding processes, thermal simulation is a very attractive method for assessing candidate steels because of its capability to reproduce a wide range of thermal cycles (welding conditions). This eliminates some of the challenges associated with the evaluation of actual pipe welds. However, it cannot replace such evaluations or the necessary requirement for formal weld qualification testing [19-21]. For successful pipeline design and construction, selection of suitable pipe steels and appropriate welding consumables for demanding applications, to meet the required level of weld metal overmatching together with adequate ductility and good low temperature toughness becomes a challenge as the strength of the pipe increases. This challenge increases with the use of high-productivity advanced gas metal arc welding using pulse (GMAW-P) processes that are known to increase the cooling time and for multi-wire systems that can result in complex thermal cycles (histories).

The objectives of this investigation were (i) to study the continuous cooling transformation (CCT) behaviours of the grain coarsened (GC) HAZ of three X100 pipe steels and an X80 pipe

[1] Gleeble® is a registered trademark of Dynamic Systems Inc. Corporation New York P.O. Box 123, Route 355 Poestenkill New York 12140

steel of similar composition using dilatometry in conjunction with optical and scanning electron microscopy, and detailed microhardness testing and (ii) to provide an evaluation of notch toughness (Charpy V-notch (CVN) transition behaviour) for a range of simulated GCHAZ and reheated HAZ regions found in pipeline girth welds.

2 EXPERIMENTAL PROCEDURES

2.1 Pipe Materials and Girth Welds

Three different commercially produced (straight seam double submerged arc welded) X100 (Grade 690) pipe steels and a modern X80 pipe material were selected for this study. The pipes ranged from 36 to 48 in. (914 to 1219 mm) diameter with wall thicknesses from 0.465 to 0.750 in (11.8 to 19.05 mm). All specimens from the respective pipes were identified to simplify tracking: X100-2, X100-5, X100-4, or X80.

Two series of rolled girth welds that made in large diameter (914 mm), thick wall (19.05 mm) X100 pipe (equivalent to X100-5 pipe) using a solid electrode wire and automated single and dual torch GMAW-P procedures were available for initial assessment of HAZ regions. For both single and dual torch welding the pipe was rotated to simulate vertical down welding. This allowed nearly identical welding parameters to be achieved for the full circumference of the pipe. For dual torch welding, the spacing between the torches was fixed at 4.75 in. (~121 mm). A minimum preheat temperature of 100ºC and maximum interpass temperature of 125ºC were used and closely monitored throughout welding. Thermal cycle data were also acquired, using a large number of thermocouples placed in predrilled holes to target the HAZ close to the fusion line, or by plunging them into the weld pool of selected fill passes. The welds were sectioned at the thermocouple locations and prepared for metallographic analysis [4, 6, 11].

2.2 Thermal Simulation and Testing Procedures

Large numbers of Gleeble® specimen blanks for dilatometric and toughness testing were cut parallel to the pipe axis from each of the X100 and X80 pipes with all specimens centered near the mid-wall of the respective pipes. The blanks were subsequently machined to size (10 x 10 x 76 mm). Two Gleeble® thermal simulators (Models 2000 and 3800) were used during this study to produce simulated HAZ microstructures and evaluate phase transformations associated with single and dual torch welding. The first step was to establish realistic thermal cycles for a range of welding process/procedure conditions with particular emphasis on GMAW-P welding. A series of Rykalin 3D cooling curves were generated to simulate the GCHAZ regions formed over a range of cooling times ($\Delta t_{800\text{-}500}$ ~1 to 50s) and these were used to develop continuous cooling transformation (CCT) diagrams for the GCHAZ using a heating rate of 300 or 500°C/s to a peak temperature of 1350°C with a 1s hold and the specific cooling times shown in Table 1. The thermal cycles incorporated an effective preheat of 100°C to closely match the welding conditions employed in making the experimental baseline welds. The specimens for dilato-metric analysis were reduced at mid-length to a cylinder of 6 mm diameter over a 6 mm length. To achieve very short cooling times that would favour martensite formation, a few specimens were reduced to a 4 mm diameter over the 6 mm length. The radial expansion and contraction of the steel was monitored with a linear variable differential transformer (LVDT) supplied with the

Gleeble® thermal simulator. The LVDT was placed at the exact mid length of the reduced section. Thermal control was maintained via a Type K thermocouple welded to the surface of the specimen. The expansion/contraction of the steel was recorded as a function of temperature during the test. Transformation temperatures were obtained from the dilatation curves and subsequently plotted as GCHAZ CCT diagrams. The majority of the thermal cycles were selected to reflect the GMAW-P parameters and focus on shorter cooling times, while longer times were used to establish the transformation behaviours of the steels over a wider range of welding conditions.

Table 1 provides complete details of the simulation conditions used to prepare specimens for toughness testing of selected simulated HAZ regions. This also included an assessment of the pipe steels along with two single-cycle simulated GCHAZs with cooling times $\Delta t_{800\text{-}500}$ = 6 and 10s, an intercritically reheated ICRGCHAZ (10% Ac_3) and an interrupted (NTR)-ICRGCHAZ where the first cycle transformation was interrupted after 50% transformation and reheated to Tp_2 = 10% Ac_3. The specimen blanks were cycled and subsequently reduced to specification (10 x 10 x 55 mm) and notched through thickness to assess properties transverse to the pipe axis (TPA). Each specimen was held in water cooled solid copper blocks with a pressure fit to ensure optimal heat conduction. It is important to note that the free span between the grips was set and maintained at 15 mm, optimized during initial testing. A total of 15 specimens were thermally cycled for each condition to allow full transition curves to be generated by testing triplicate specimens over a range of temperatures.

2.3 Metallography, Microhardness Testing and Fractography

The CCT samples were prepared for metallographic analysis by removing the 6 mm long reduced section of the specimen and cutting 2 mm away from the centrally located thermocouple. The section was then mounted under vacuum in clear epoxy. The samples were ground flush to the thermocouple plane to guarantee correlation of the thermal cycle and the microstructure. Grinding and polishing were achieved using diamond suspensions to a size of 1 μm followed by a final colloidal silica polish of 0.05 μm. Samples were etched using a 3% Nital solution for 8-12 seconds. The microstructures were examined using an optical microscope at a range of magnifications. Microhardness traverses were made using a Clemex micro hardness indenter at 300 gram force; the values reported in the CCT diagrams are the average of a minimum of ten indents. The microstructural features of selected samples and the fracture surfaces of broken GCHAZ Charpy specimens were examined using scanning electron microscopy in a JEOL JCM-500 NeoScope.

3 RESULTS

3.1 Pipe Materials

The large-diameter pipes used were made from low-alloy thermo-mechanical-controlled process (TMCP) steels with a specified minimum yield strength of 690 MPa (100 ksi) and 550 MPa (80 ksi). Table 2 summarizes the compositions, carbon equivalents and bainite and martensite start temperatures calculated as proposed by Steven and Haynes [22]. All four pipe steels have similar C and Mn contents and are based on variations of the Ni-Mo-Cr-Cu-Nb-Ti alloying

system. The X100-2 pipe steel exhibits the lowest hardenability, as reflected by the calculated carbon equivalents. The X100-5 pipe steel higher nickel content with lower niobium and very low nitrogen, while the X100-4 pipe steel has increased additions of Ni, Cr, Cu, but low Nb and N compared to X100-2. The X80 pipe steel has high Cr and Nb contents with comparatively low carbon equivalents values.

Figure 1 shows representative micrographs for the pipe steels. The microstructures of X100-2 and X100-5 consisted of fine bainite and martensite with occasional polygonal ferrite. In the latter case, significant banding is apparent in the microstructure owing to the steelmaking and thermo-mechanical processing used in steel production. The banding was examined and reported in more detail in a companion report [7]. The microstructure and hardness varied within the X100-5 pipe steel and this was linked to significant differences in proportions of bainite (286 HV) and martensite (369 HV) in the microstructure. In contrast, a more uniform predominantly bainitic structure with occasional polygonal ferrite was observed in the X100-4 pipe steel. The markedly different structure of the X80 pipe steel, in Figure 1(d), was dominated by an acicular ferrite/bainite with polygonal ferrite microstructure.

3.2 Dilatometric Data Analysis

Volumetric expansion and contraction is associated with thermal strain and phase transformations. Dilatation curves were examined to establish the transformation start (T_s) and finish (T_f) temperatures based on deviation from linearity for the FCC decomposition and resultant transformation products [23-25]. Other temperatures such as the point of major transformation start (T_3) based on an offset of ~3% were also determined as were any obvious inflection points where both austenite and its transformation products co-existed. For the X100 and X80 pipe steels, a few samples were cooled very quickly ($\Delta t_{800\text{-}500}$ = 2s) in an attempt to develop fully martensitic microstructures and determine the respective martensite start (M_s) temperatures. Dilatation curves in Figure 2 indicate that the major onset of transformation occurred at temperatures between 450 and 500°C for all three X100 pipe steels. The transformation start temperature is slightly lower for the X100-4 compared to X100-2 steel. For the X100-5 pipe steel, the curve is more rounded and deviation from linearity begins above 500°C, indicating that a small transformation (to bainite) occurs before the M_s is reached. The major transformation for the X80 pipe steel is closer to 500°C, and using the predicted M_s of 470°C as a guide, a significant fraction (~50%) of bainite is expected to form before the M_s is reached. Representative micrographs of the GCHAZ formed with the short cooling time ($\Delta t_{800\text{-}500}$ = 2s), are shown in Figure 3. Almost-fully-martensitic structures are seen for both X100-2 and X100-4, whereas a small amount of bainite formed along with martensite in X100-5 (Figure 3(b)). In agreement with the dilatation curve, the GCHAZ structure of the X80 pipe steel contains regions of both fine and relatively coarse bainite regions along with some low-carbon lath martensite (Figure 3(d)).

3.3 CCT Diagrams, Microstructure and Hardness

CCT diagrams constructed for the GCHAZ are presented along with representative micrographs showing the microstructures formed at cooling times $\Delta t_{800\text{-}500}$ = 6, 10, 30 and 50s in Figure 4 through Figure 11. Table 4 lists the average, range, and standard deviations of the microhardness

values, which give a good indication of the observed variations and the trend towards lower hardness with increasing cooling times. From these data, it is evident that X100-5 had the largest standard deviation, whereas X100-4 had the most uniform results at the shorter cooling times. Figure 12 shows plot of average GCHAZ microhardness versus cooling time for the four pipe steels. There is marked decrease in GCHAZ hardness observed for the initial cooling times ($\Delta t_{800\text{-}500} \leq 10$s) for all pipe steels, except X100-4. The GCHAZ of the X100-4 steel has lower initial hardness (shortest cooling time) and decreases much more gradually and then generally parallels the other curves, but at higher overall microhardness levels. It is apparent from examination of the series of micrographs presented here that all simulated GCHAZ samples formed microstructures with varying proportions of lath martensite, fine bainite, upper bainite and/or granular bainite within the prior austenite grain interiors. Also evident is the relatively wide range of prior austenite grain sizes and a tendency for increasing grain size with longer cooling times.

For the X100-2 pipe steel, the GCHAZ CCT (Figure 4) indicates formation of relatively high hardness (360 HV), predominantly martensitic structure at the shortest cooling times. There are higher proportions of bainite with further decreases in hardness at intermediate cooling times that continue to decrease gradually for the longest cooling times ($\Delta t_{800\text{-}500}$ = 30 and 50 s, 250 and 235 HV, respectively). Several packets containing bainitic ferrite laths of similar orientation can also be seen within an individual prior austenite grain, as evident in Figure 5. The GCHAZ CCT diagram for X100-5 reveals a smaller range over which both martensite and bainite are formed that is consistent with the observed microstructures (Figure 3(b) and Figure 7) and the greater range of microhardness values. Similar to X100-2, coarser mainly bainitic structures were found at the longer cooling times. In this case, formation of martensite-austenite (M-A) constituent phases between the bainitic ferrite laths can be seen in Figure 7(c) and (d). The situation is quite different for the more highly alloyed X100-4 pipe steel as revealed in the GCHAZ CCT diagram in Figure 8. Formation of much finer microstructures over the complete range of cooling times, combined with a more gradual decrease in microhardness (remaining above 300 HV for $\Delta t_{800\text{-}500} \leq 17$ s) is consistent with the comparatively low transformation temperatures and the resultant microstructures in Figure 9. High proportions of low carbon lath martensite are initially formed at the shorter cooling times (high cooling rates), while at intermediate times fine bainite forms at the expense of martensite. Note the small rise in transformation temperature and formation of fine bainite even at the longest cooling times, $\Delta t_{800\text{-}500}$= 30 and 50 s. Although the X80 pipe steel has a carbon equivalent between the two leaner X100 pipe steels, it exhibited higher T_s temperatures (above 500°C). Even for the shortest cooling times a fully martensitic structure was not developed. From the CCT diagram in Figure 10, transformation to bainite extends completely across the entire range of imposed thermal cycles (range of cooling times). Lower hardnesses are related to formation of more bainitic microstructures (Figure 3(d) and Figure 11), especially at the longer cooling times where the bainitic ferrite laths are seen to be coarser. From the selected dilatometric data in Table 3, relative differences in transformation temperatures (T_s, $T_{\sim 3}$ and T_{50}) with increasing cooling time for all four pipe steels are revealed and can be compared to the calculated B_s and M_s temperatures that are also provided. Reasonably close agreement is seen for $T_{\sim 3}$ offset temperature and the calculated M_s for the X100 pipe steels. The same is not true for the B_s temperatures, which represent transformation to a fully bainitic structure, where only the X80 pipe steel shows reasonable correlation.

In addition to the simulated single-cycle GCHAZ microstructures described above, selected double cycled HAZ regions were also included in this evaluation (Table 1). Representative micrographs of the double-cycle ICR-GCHAZ and NTR-ICR-GCHAZ regions formed in the X100-05 and the X80 pipe steels are presented in Figure 13 and Figure 14, respectively. For the ICR-GCHAZ simulation conditions used for the X100-5 pipe steel (Tp1=1350°C hold for 1 s followed by $\Delta t_{800\text{-}500}$= 6s down to 150 °C followed by second reheat at 250°C/s to 10% of the Ac_3 (770°C), holding for 2 s followed by $\Delta t_{800\text{-}500}$= 12s), it can be seen that prior austenite grains are decorated by a discontinuous second phase, while a relatively coarse predominately bainitic structure exists within the grain interiors. This structure is consistent with the partial reaustenization and comparatively longer cooling time $\Delta t_{800\text{-}500}$= 12s of the second cycle. In contrast, the interrupted (dual torch) NTR-ICR-GCHAZ exhibits a microstructure that resembles the single cycle GCHAZ (Figure 13(c)). The images in Figure 14 reveal similar features for the HAZ regions formed in the X80 pipe steel, although there is much more complete delineation of the prior austenite grain boundaries and a mixed microstructure with coarse bainite within the grain interiors for the ICR-GCHAZ. The structure of the NTR-ICR-GCHAZ (Figure 14) contains relatively large and coarse upper or granular bainite packets along with some finer regions.

3.4 Charpy Impact Toughness

The results of Charpy impact tests obtained for the pipe steels and corresponding simulated HAZ regions are listed in Table 5 to Table 8, while full transition curves are presented in Figure 15 through Figure 19. The transition curves were fit using a hyperbolic tangent function with best fit for the lower and upper shelf energies as well as the span and transition temperature. From the detailed information in these tables it can be seen that in a few instances there was considerable scatter in the absorbed energies and measured percent shear values. Toughness of the pipe steels was very good with high absorbed energies recorded at temperatures at or above -40°C. It is worth pointing out that varying amounts of splitting were observed on the fracture surfaces of several of the pipe steel Charpy specimens, as indicated in the tables. All four pipe steels exhibited high upper shelf energies at -20°C and displayed a range of energy transition temperatures (ETT) between -98 and -46°C. The ETT represents the temperature corresponding to the average between the lower and upper shelf energies. The X100-4 pipe steel exhibits the lowest ETT followed by X100-2, X100-5 and X80, as shown in Figure 15 and Table 9. For both X100-2 and X100-4 pipe steels the lower shelf was not reached even at the very low test temperature of -120ºC.

Comparisons of the impact toughness transition behaviour of the respective pipe steels and the simulated HAZ regions are provided in Figure16 to Figure 19, while a summary of the results is listed in Table 9. As expected, the transition curves are shifted towards higher temperatures for the HAZ simulation conditions investigated. For the X100-2 pipe steel, there is a shift in transition for both single-cycle GCHAZ regions, although the performance of GCHAZ-6s remains very good. Some scatter was observed for the GCHAZ-10s tested at -20°C and an unexplained increase in toughness occurred for the -40°C test temperature; however there is a general trend of lower toughness with increasing cooling time. The pipe steel X100-5 simulated-HAZ transition curves are dramatically shifted towards higher temperatures, as shown in Figure 17. From Table 9, the increase in ETT and marked decrease in absorbed energies for tests

conducted at -20°C and -60°C occurs for all of the HAZ simulation conditions. Progressively lower toughness is seen for single-cycle GCHAZ and ICRGHAZ samples, whereas the NTR-ICRGCHAZ is generally better than the GCHAZ-10s and the ICRGCHAZ. Although there is a shift in the transition curves toward higher temperatures for the simulated HAZ regions produced in the X100-4 pipe steel, high toughness is seen for the
-20°C test temperature (Figure 18). Interestingly there was very little difference between the single-cycle simulated GCHAZs, which had ETT of -50°C, while the ICRGCHAZ is shifted upwards by another 10°C to -40°C.

Toughness results for the X80 pipe steel (Figure 19 and Table 9) show similar trends with a shift in transition relative to the pipe steel for all simulated HAZ samples. The ETTs are all equal to or above -18°C. For GCHAZ-6s, the average energy of 84 J may not be truly representative since there was considerable scatter (Table 8) and a large variation in percent shear (0 to 55%). The very similar results obtained for both ICRGCHAZ and the NTR-ICRGCAHZ produce a further increase in the ETT to -6 and -4°C, respectively.

3.5 Fractographic Analysis

Examination of the fracture surfaces of the single-cycle simulated GCHAZ was carried out using SEM for selected specimens broken at low temperature to allow the fracture appearance and possible initiation sites to be characterized. Figure 20 through Figure 25 show the series of fractographs for the X100 pipe steels. In all cases considerable variations in cleavage facet size and differences in the length and severity of secondary cracks is observed. In some cases, the fracture initiation site could be found.

Figure 20 and Figure 21 show the range of cleavage facet sizes observed for X100-2 simulated GCHAZ samples. In this case, it is seen that relatively fine equiaxed or elongated facets appear to dominate, while in other locations comparatively large flat cleavage facets can be seen as in Figure 20(b) and (d) as well as in Figure 21. The change in facet shape and size is related to the mixed martensitic/bainitic microstructures formed in the GCHAZ regions. It has been shown for martensitic and bainitic GCHAZ structures that the packet size corresponds closely with the cleavage facet dimensions. The elongated facets are believed to be associated with low carbon lath martensite or intragranularly nucleated bainite regions, whereas the larger more equaixed facets are associated with coarser bainite packets, which offer little resistance to crack propagation [13, 14].

Figure 22 and Figure 23 show some unique fracture features observed for the X100-5 simulated GCHAZ-6s and 10s samples. From this series of images, it is clear that coarser cleavage facets dominate with some large flat facets also evident. Both GCHAZ samples revealed initiation from microstructural features or non-metallic inclusions (Figure 22 (a-c) and Figure 23(b)). There was an increased frequency of secondary microcracks extending over long distances sometimes equal to the prior austenite grain size. It is also important to notice the presence of several aligned intragranular facets and the obvious microcracking along the prior austenite grain boundaries, as shown in Figure 23(d).

Examination of the X100-4 simulated GCHAZ samples revealed a higher fraction of finer more elongated cleavage facets, although it was possible to find occasional large flat facets as indicated in Figure 24(d) and Figure 25(a)). Again, inclusions were present at initiation sites within the facets shown in Figure 24(c) and 24(d)). The inset images in both figures confirm that cleavage fracture initiated from inclusions. Also notice the comparatively large flat facet and long transgranular secondary microcrack in Figure 24(d).

4 DISCUSSION

In this investigation, the continuous cooling transformation behaviour of simulated GCHAZ regions formed in three X100 pipe steels and a modern X80 pipe steel of similar composition was established. Further evaluation of the Charpy impact toughness of different GCHAZ and ICR-GCHAZ regions produced using thermal simulation techniques was also carried out to establish the intrinsic properties of the pipe steels investigated. Development of CCT diagrams applicable to the GCHAZ region formed over a wide range of cooling times relevant to pipeline girth welding, especially the relatively fast cooling conditions associated with mechanized single and dual torch GMAW-P process variants has been successfully completed. Evaluation of the HAZ notch toughness properties using both single and double thermal cycles that were created to closely match the regions observed in actual girth welds (Figure 26) has led to better understanding of the factors influencing HAZ performance and allows the pipe steels to be ranked and compared. Achieving good agreement between the simulated and actual weld GCHAZ microstructure is important for Gleeble® specimens used for Charpy impact testing [24]. One important limitation of thermal simulation relates to the fast cooling conditions that are known to exist for low-energy-input welding. Measurement of thermal cycles was part of the current program and has been documented by other researchers [4, 6, 17, 19]. For example, very short cooling times of the order of $\Delta t_{800\text{-}500}$ = 2 to 4 s were measured for a single torch welding procedure [19], whereas significantly longer times were recorded for a dual torch procedure ($\Delta t_{800\text{-}500}$ = 9 s). These data were also in reasonably good agreement with the results from the thermal simulation model developed in this program [4]. With this information, the Gleeble® simulation experiments were designed to use T_p=1350°C and the shortest cooling time possible, i.e. $\Delta t_{800\text{-}500}$ = 6 s, with a free span (distance between the copper grips) of 15 mm. The second cooling time, $\Delta t_{800\text{-}500}$ = 12 s, was chosen to represent the thermal cycle of a dual torch or high preheat/interpass welding condition.

4.1 CCT Diagrams, Microstructure and Hardness

The CCT diagrams, which were constructed from analysis of dilatometric data and evaluation of the corresponding simulated GCHAZ microstructures, reveal some interesting trends. Formation of martensite along with various morphologies of bainite occurs with increasing cooling times, consistent with the observed decrease in microhardness (Figure 12) for the range of pipe compositions (relative hardenability) investigated. Three out of the four pipe steels exhibited marked decreases in hardness for cooling times $\Delta t_{800\text{-}500} \leq 10$ s. In contrast, a more gradual decrease occurs for the X100-4 GCHAZ regions, which is consistent with transformation to finer overall microstructures over the complete range of cooling times and accounts for the higher levels of microhardness.

The observed differences in the specific GCHAZ microstructures (proportions of martensite and bainite) can, in part, be explained on the basis of the pipe steel hardenabilities (carbon equivalents) and resultant transformation start temperatures. For example, the X100-4 and X80 exhibit markedly different microstructures related to the transformation temperatures, which is reflected in the proportion of lath martensite formed in the respective pipe steel GCHAZ regions. This is consistent with the dilatation curves in Figure 2 for a thermal cycle with a short cooling time $\Delta t_{800\text{-}500} \sim 2$ s. For the other two X100 steels, there are differences in GCHAZ microstructures, including formation of greater amounts of bainite in the case of X100-5 pipe steel which is readily apparent in Figure 5 and Figure 7, and that is consistent with the change in microhardness (Table 4).

4.2 Toughness of Simulated HAZ regions

Assessment of the notch toughness and transition behavior for the simulated GCHAZ-6s and GCHAZ-10s reveals significant differences for the range of pipe steels investigated. It is important to recognize that the evaluation of simulated HAZ regions provides an excellent method for comparing and/or ranking the pipe steels and eliminates complications associated with the evaluation of real welds where complex distributions of HAZ regions and narrow width of the HAZ are often encountered. From the transition curves and the toughness results summarized in Table 9, it is clear that the highest-alloyed pipe steel X100-4 (CE = 0.55 and CEN=0.30) exhibited the best overall toughness. This can be correlated with the higher proportions of low-carbon lath martensite along with finer bainite that formed at cooling times $\Delta t_{800\text{-}500} \leq 10$s (Figure 8) from suppression of the $\gamma \rightarrow \alpha$ transformation to lower temperatures. The transformation temperatures (T_s and T_{50}) recorded in this study (Table 3) are in very close agreement with those found by Hara et al. [15] for two X100 pipe steels; one similar to the pipe used in this study and another alloyed with Mo. Interestingly, the GCHAZs obtained by thermally cycling the steels to a T_p =1400°C, holding for 1s and continuously cooling at rates between 60°C/s and 10°C/s had very similar transformation temperatures.

On the other hand, there is a decrease in toughness for the X100-2 and X100-5 simulated GCHAZ regions that relates to the differences in microstructure, despite their similarity in microhardness. The increasing proportions of coarse bainite found in the X100-5 GCHAZ regions (Figure 7) accounts for the inferior notch toughness. This is also the case for the X80 GCHAZ where similar toughness levels were observed. SEM examination of the cleavage fractures revealed that the high toughness was associated with finer more elongated facets (Figure 21, 22, 23 and 24), although occasional large flat facets may also exist, as evidenced in Figure 21(b) and 24(d). In both cases, initiation occurred from microstructural features or non-metallic inclusions. For the X100-5 pipe steel, a much more coarse faceted fracture appearance was found with more frequently observed secondary microcracking. The presence of intragranular facets, which are known to reduce toughness, was confined to the middle region of the broken Charpy specimen (mid-wall of the pipe where ferrite and high-hardness martensite exist); HAZ simulation resulted in both cleavage and intragranular fracture modes.

The further reduction in toughness for the ICRGCHAZ region was believed to be caused by formation of secondary phase that decorated the prior austenite grain boundaries [14]. However,

further work is required to fully understand the influence of the extended cooling time $\Delta t_{800\text{-}500} \leq$ 12 s compared with the range of cooling times that are expected to occur for small changes in welding conditions. In contrast, the NTR-ICRGCHAZ regions (X100-5 and X80) that were created using an interrupted transformation (50%) and subsequent reheat to the two phase region (10% Ac_3) was not as deleterious as the fully transformed ICRGCHAZ. The incomplete transformation coupled with subsequent intercritical reheating did not change the microstructures as much.

Finally, although it is possible to show clear trends in terms of transformation and notch toughness behaviours for the pipe steels investigated, because of the very fine microstructural features of the simulated HAZ regions it is recommended that more advanced characterization techniques be used to fully understand the factors responsible for the observed microstructure and property relationships.

5 CONCLUSIONS

In this investigation, the transformation behaviours of simulated GCHAZ regions formed in three X100 pipe steels and a modern X80 pipe steel of similar composition were established. Charpy notch toughness of specimens with simulated GCHAZ and ICR-GCHAZ regions was evaluated. The following conclusions have been drawn from this work:

1. CCT diagrams applicable to the single-cycle GCHAZ region, using T_p=1350°C with a 1 s hold and cooling times $\Delta t_{800\text{-}500}$ = 1.2 to 50 s, have been constructed for three X100 pipe steels and a modern X80 pipe steel of similar composition. The differences in transformation temperatures, determined from analysis of dilatometric data, were dependent on the pipe steel composition and imposed thermal cycle (cooling time).
2. GCHAZ microstructures with varying proportions of lath martensite and different morphologies of bainite were found with increasing cooling time. These changes and the overall coarsening of the transformed microstructures are consistent with the reduction in hardness for a given the pipe steel composition (hardenability). Interestingly, the GCHAZ regions of the highest alloyed X100-4 exhibited lower initial hardnesses that gradually decreased with increasing cooling times compared to the other pipe steels.
3. Thermal cycles were created to facilitate simulation of single-cycle GCHAZ, double cycle ICR-GCHAZ, and a NTR-ICR-GCHAZ (with interrupted first cooling cycle) and used to produce Charpy impact specimens for testing (using a through-thickness notch and LPA specimen orientation) and comparison of impact properties of HAZs with the respective pipe steels.
4. A trend of decreasing notch toughness (reductions of absorbed energies and shift in energy transition temperatures) was found for the simulated HAZ regions compared with the respective pipe steels. From this data it was possible to establish a descending ranking of HAZ toughness as follows: X100-4, X100-2, X100-5 and X80. The pipe steel (X100-4) with the highest hardenability resulting from additions of Ni, Cr (instead of Mo), Cu and lower Nb with optimum Ti and N exhibited the best pipe steel and HAZ toughness. This can be correlated with the formation of more favourable lath martensite along with fine bainite microstructures as a result of the suppression of the $\gamma \rightarrow \alpha$ transformation to lower temperatures.

5. For the X100 pipe steel,GCHAZ regions both narrow elongated and larger diameter flat cleavage facets were observed and were assumed to correspond with the packet size of fine lath martensite/bainite and coarser bainitic region, respectively.
6. The lower toughness exhibited by the X100-5 and X80 GCHAZ regions is attributable to the formation of higher proportions of coarse bainite, which provide lower resistance to crack propagation as evidenced by large cleavage facets on the fracture surfaces.
7. In some cases initiation of cleavage fracture was linked to specific microstructural features or non-metallic inclusions.
8. Further deterioration of toughness was observed for the ICRGCHAZ and ascribed to partial re-austenization and subsequent transformation of microphase at the prior austenite grain boundaries. For the NTR-ICR-GCHAZ, the slightly better toughness relative to the ICR-GCHAZ is related to the formation of greater proportions of austenite and subsequent transformation as a result of the longer cooling time $\Delta t_{800\text{-}500} = 12$ s.

6 ACKNOWLEDGEMENTS

This research was funded by CANMET-MTL and the Federal Interdepartmental Program for Energy Research and Development. The authors would like to thank Mr. M. Kerry for his machining expertise, Mr. R. Eagleson for mechanical testing, and Ms. P. Liu for contributions to metallographic analysis and microhardness testing. The research is part of a larger consolidated program jointly funded by the Pipeline and Hazardous Materials Safety Administration of the U.S. Department of Transportation (DOT), and the Pipeline Research Council International, Inc. (PRCI). The views and conclusions in this paper are those of the authors and should not be interpreted as representing the official policies of any of these organizations.

The author (GG) also wishes to acknowledge CANMET-MTL management for providing the opportunity to work and have access to laboratory facilities during the course of this research and to NSERC and McGill University for funding grants.

7 REFERENCES

1. DOT-PRCI, "Update of Weld Design, Testing, and Assessment Procedures for High Strength Pipelines," http://primis.phmsa.dot.gov/matrix/PrjHome.rdm?prj=225, 2007-2011.
2. DOT-PRCI, 2007 "Development of Optimized Welding Solutions for X100 Linepipe Steel," http://primis.phmsa.dot.gov/matrix/PrjHome.rdm?prj=226, 2007-2011.
3. Gianetto, J., Goodall, G.R., Tyson, W.R., Quintana, M.A., Rajan, V.B. and Chen, Y., "Microstructure and Properties of Simulated Weld Metals", Final Report 278-T-04 to PHMSA per Agreement # DTPH56-07-T-000005, September 2011.
4. Chen, Y., Wang, Y-Y., Quintana, M.A., Rajan, V.B. and Gianetto, J.A., "Thermal Model for Welding Simulations", Final Report 278-T-07 to PHMSA per Agreement # DTPH56-07-T-000005, September 2011.
5. Chen, Y., Wang, Y-Y., Quintana, M.A., Rajan, V.B. and Gianetto, J.A., "Microstructure Model for Welding Simulations", Final Report 278-T-08 to PHMSA per Agreement # DTPH56-07-T-000005, September 2011.
6. Panday, R. and Daniel, J., "Materials Selection, Welding and Weld Monitoring", Final Report 278-T-02 to PHMSA per Agreement # DTPH56-07-T-000005, September 2011.
7. Gianetto, J.A., Goodall, G.R., Tyson, W.R., Quintana, M.A., Rajan, V.B and Chen, Y., "Microstructure And Hardness Characterization Of Girth Welds", Final Report 278-T-03 to PHMSA per Agreement # DTPH56-07-T-000005, September 2011.
8. Gianetto, J.A., Tyson, W.R., Park, D.Y., Shen, G., Lucon, E., Weeks, T.S., Quintana, M.A., Rajan, V.B. and Y.-Y. Wang, "Small Scale Tensile, Charpy V-Notch, and Fracture Toughness Tests", Final Report 277-T-05 to PHMSA per Agreement # DTPH56-07-T-000005, September 2011.
9. Park, D.Y., Tyson, W.R., Gianetto, J.A., Shen, G., Eagelson, R., Lucon, E. and Weeks, T.S., "Development of Optimized Welding Solutions for X100 Line Pipe Steel-Small Scale Low Constraint Fracture Toughness Test Results", Final Report 277-T-06 to PHMSA per Agreement # DTPH56-07-T-000005, September 2011.
10. Park, D.Y., Tyson, W.R., Gianetto, J.A., Shen, G., Eagelson, R., , E. and Weeks, T.S., "Development of Optimized Welding Solutions for X100 Line Pipe Steel-Small Scale Low Constraint Fracture Toughness Test Discussion and Analysis", Final Report 277-T-07 to PHMSA per Agreement # DTPH56-07-T-000005, September 2011.
11. Rajan, V.B., "Essential Welding Variables", Final Report 278-T-09 to PHMSA per Agreement # DTPH56-07-T-000005, September 2011.
12. Harrison, P.L., and Farrar, R.A., "Application of continuous cooling transformation diagrams for welding of steels," International Materials Reviews, Vol. 34 No.1 pp. 35-51, 1989.
13. Bowker, J.T., McGrath, J.T., Gianetto, J.A. and Letts, M.W., " The Effect of Composition on the Heat Affected Zone Microstructure and Toughness of HSLA Steel" Proceeding of International Conference Welding-90: Technology, Materials, Fracture Ed. M. Kocak, pp. 211-218, 1990.
14. Lambert-Perlande, A., Gourgues, A.F., Besson, J., Strurel, T. and Pineau, A., "Mechanisms and modeling of Cleavage Fracture in Simulated Heat-Affected Zone

Microstructures of a High-Strength Low Alloy Steel", ASME, Metallurgical and Materials Transactions A, Vol. 35A, No. 3, pp. 1039- 1053, 2003.

15. Shome, M. Gupta, O. P. and Mohanty, O. N., "Effect of Simulated Thermal Cycles on the Microstructure of the Heat-Affected Zone in HSLA-80 and HSLA-100 Steel Plates," Metallurgical and Materials Transactions A, Vol. 35A, pp. 985-996, 2004.
16. Penniston, C., Collins, L., and Hamad, F. "Effects of Ti, C and N on Weld HAZ Toughness of High Strength Line Pipe," 7th Int. Pipeline Conf., ASME, IPC2008-64134, pp.1-9, 2008.
17. Hara, T., Terada, Y., Shinohara, Y., Asahi, H., and Doi, N. 2008 "Metallurgical Design and Development of High Deformable X100 Line Pipe Steels Suitable for Strain-Based Design," 7th Int. Pipeline Conf., ASME, IPC2008-64234, pp.1-7.
18. Onsoien, M.I., M'Hamdi, M., and Mo, A., "A CCT Diagram for an Offshore Pipeline Steel of X70 Type," The Welding Journal, Vol. 88, No. 1, pp 1s-6s, 2009.
19. Hudson, M., 2004 "Welding of X100 Linepipe", PhD Thesis in School of Industrial and Manufacturing Science, Cranfield University: Bedfordshire. p. 330.
20. Hukle, M. W., Lillig, D. B., Newbury, B. D., Dwyer, J. and Horn, A. M. "Development and Qualification of Pipeline Welding Procedures for Strain Based Design," in International Conference on Offshore Mechanics and Arctic Engineering (OMAE), San Diego, California, USA, 2007, pp. 217-223.
21. Hamad, F., Collins, L., and Volkers, R. 2008 "Effects of GMAW Procedure on the Heat-Affected Zone (HAZ) Toughness of X80 (Grade 550) Linepipe," 7th Int. Pipeline Conf., ASME, IPC2008-64097, pp.1-17.
22. Steven, W. and Haynes, A. G. 1956 "The Temperature of Formation of Martensite and Bainite in Low-Alloy Steels," Journal of Iron and Steel Research International.
23. Goodall, G.R., Voyzelle, B., Bowker, J., and Brochu, M., 2011 "Comparison of Base Metal and HAZ CCT Diagrams for X100 Pipe Steel" CANMET Materials Technology Laboratory Report 2011-10(TR-R), Thesis Manuscript, McGill University.
24. Goodall, G.R., Gianetto, J.A, Bowker, J., and Brochu, M., 2011 "CCT Diagrams and Impact Toughness Applicable to the GC HAZ Region Generated in X100 Line Pipe" CANMET Materials Technology Laboratory Report 2011-11(TR-R), Thesis Manuscript, McGill University.
25. Goodall, G.R., Gianetto, J.A, Bowker, J., and Brochu, M., 2011 "Thermal Simulation of HAZ Regions in a Modern High Strength Steel," CANMET Materials Technology Laboratory Report 2011-13(TR-R), Thesis Manuscript, McGill University.
26. Lundin, C.D. and Zhou, G., 2000 "Comparison of Published HAZ Thermal Simulation Methods Used to Derive Weld HAZ Thermal Cylces," Acta Metallurgica Sinica, Vol. 13, No. 1, pp. 223-232.

Table 1. Details of thermal cycle conditions used for single and dual cycles

Single Thermal Cycles	Simulation Parameters
GCHAZ CCT study	Heat at 300-500°C/s to 1350°C, hold for 1 s, followed by cooling times $\Delta t_{800-500}$= 1.2, 2, 3, 5, 7, 10, 16, 20, 25, 30 and 50 s
GCHAZ Charpy Specimens	Heat at 300-500°C/s to 1350°C, hold for 1 s, followed by cooling times $\Delta t_{800-500}$= 6 and 10 s.
Double Thermal Cycles	**Simulation Parameters**
ICR-GCHAZ – X100-5	Heat at 500°C/s to 1350°C hold for 1 s, followed by $\Delta t_{800-500}$= 6s to 150 °C, heat at 250°C/s to 10% of the Ac_3 (770°C), hold for 2 seconds followed by $\Delta t_{800-500}$= 12 s
NTR-ICR-GCHAZ –X100-5	Heat at 500°C/s to 1350 °C, hold for 1 s, followed by $\Delta t_{800-500}$= 6s to 50% of the measured Ar_3 (455°C), heat at 250°C/s to 10% of the Ac_3 (770°C), hold for 2 s followed by $\Delta t_{800-500}$= 12 s
ICR-GCHAZ –X100-4	Heat at 500°C/s to 1350°C hold for 1 s, followed by $\Delta t_{800-500}$= 6s to 150 °C, heat at 250°C/s to 10% of the Ac_3 (800°C), hold for 2 seconds followed by $\Delta t_{800-500}$= 12s
ICR-GCHAZ –X80	Heat at 500°C/s to 1350°C hold for 1 s, followed by $\Delta t_{800-500}$= 6s to 150 °C, heat at 250°C/s to 10% of the Ac_3 (810°C), hold for 2 seconds followed by $\Delta t_{800-500}$= 10s
NTR-ICR-GCHAZ –X80	Heat at 500°C/s to 1350 °C, hold for 1 s, followed by $\Delta t_{800-500}$= 6s to 50% of the measured Ar_3 (510°C), heat at 250°C/s to 10% of the Ac_3 (810°C), hold for 2 s followed by $\Delta t_{800-500}$= 12 s

Note: 10% of Ac_3 refers to the temperature at which 10% austenite is formed on reheating between Ac_1 and Ac_3.

Table 2. Chemical compositions of X100 and X80 pipe steels

Element Wt%	X100 Pipe Steel			X80 Pipe
	X100-2	X100-5	X100-4	X80
C	0.058	0.061	0.050	0.052
Mn	1.8	1.76	1.87	1.7
Si	0.09	0.10	0.19	0.11
S	0.001	0.002	0.001	0.003
P	0.002	0.006	0.007	0.009
Ni Cr Mo Cu	0.63	1.07	1.54	0.85
Al Nb Ti	0.073	0.079	0.044	0.141
N	0.0060	0.0025	0.0030	0.0060
Ti/N	1.67	4.8	3.33	2.33
CE_{IIW}	0.43	0.47	0.55	0.45
P_{CM}	0.18	0.20	0.21	0.18
CEN	0.27	0.28	0.30	0.28
B_s	628	612	585	626
M_s	467	459	457	470

Notes: For all steels, B= <0.0005, V=0.004

$CE_{IIW} = C + Mn/6 + (Cr+Mo+V)/5 + (Ni + Cu)/15$

$P_{cm} = C + Si/30 + (Mn+Cu+Cr)/20 + Ni/60 + Mo/15 + V/10 + 5B$

CEN=C+A(C) (Si/24+Mn/6+Cu/15+Ni/20+(Cr+Mo+Nb+V)/5+5B)

A(C)= 0.75 +0.25 tanh{(20(C-0.12)}

$B_s = 830-270(C)-90(Mn)-37(Ni)-70(Cr)-83(Mo)$

$M_s= 561-474(C)-33(Mn)-17(Ni)-17(Cr)-21(Mo)$

Table 3. Summary of dilatation data as a function of cooling time

Pipe Material	X100-2			X100-5			X100-4			X80		
Cooling Time $\Delta t_{800\text{-}500}$, s	T_s °C	$T_{\sim 3}$ °C	T_{50} °C	T_s °C	$T_{\sim 3}$ °C	T_{50} °C	T_s °C	$T_{\sim 3}$ °C	T_{50} °C	T_s °C	$T_{\sim 3}$ °C	T_{50} °C
2	500	475	455	520	485	450	476	465	450	520	502	480
10	540	515	465	550	535	465	560	540	470	585	560	515
30	580	565	510	595	575	525	570	535	495	630	615	565
Calculated Start Temperatures, °C	B_s = 628 M_s= 467			B_s = 612 M_s= 460			B_s = 585 M_s= 457			B_s = 626 M_s= 470		

Note: T_s represents first onset of transformation, whereas $T_{\sim 3}$ is the point of major transformation based on a ~3% offset from the linear contraction of austenite and T_{50} was determined using the lever rule and represents temperature for 50% transformed.

Table 4. Summary of microhardness results for CCT samples as a function of cooling time

Pipe Material	X100-2			X100-5			X100-4			X80		
Cooling Time $\Delta t_{800\text{-}500}$, s	Mean HV	Range HV	STDEV HV	Mean HV	Range HV	STDEV HV	Mean HV	Range HV	STDEV HV	Mean HV	Range HV	STDEV HV
2	360	347-378	9.7	344	311-363	15.2	336	326-344	4.4	319	310-329	6.0
6	319	306-337	9.2	308	278-346	26.8	332	322-345	6.6	288	267-304	10.4
10	300	283-312	9.6	294	244-340	32.4	323	310-333	6.8	268	255-285	10.7
20	-	-	-	-	-	-	-	-	-	247	241-263	6.9
30	250	231-267	10.0	253	233-285	19.4	282	272-303	9.2	-	-	-
50	235	228-248	7.0	238	226-254	8.9	262	246-283	10.6	228	221-245	7.2

Table 5. Charpy impact toughness of X100-2 pipe steel and simulated HAZ regions

Region ID	Test Temperature, °C	Charpy Impact Energy, J	Average Charpy Impact Energy, J	Average Shear Area %
Pipe Steel Base Metal	-20	(269, 281, 265)	272	100
	-60	(235, 274, 269)	259	100*
	-80	(192, 180, 204)	192	55-88*
	-100	(155, 58, 35)	83	31-55*
	-120	(17, 96, 23)	45	11-39
GCHAZ-6s	-20	(240, 252, 248)	247	100
	-40	(155, 250, 208)	204	70-100
	-60	(84, 24, 168)	92	17-56
	-80	(16, 58, 30)	35	11-21
GCHAZ-10s	22	(249, 267, 296)	271	100
	-5	(249, 231, 276)	252	84-90
	-20	(40, 250,167)	152	21-100
	-40	(208, 240, 210)	219	67-77
	-60	(42, 30, 42)	38	11-21

Note: *Splits were observed on the fracture surfaces

Table 6. Charpy impact toughness of X100-5 pipe steel and simulated HAZ regions

Region ID	Test Temperature, °C	Charpy Impact Energy, J	Average Charpy Impact Energy, J	Average Shear Area %
Pipe Steel BM	-20	(300, 282, 278)	287	100
	-60	(243, 246, 223)	237	88-100
	-80	(26, 40, 162)	76	16-57
	-100	(115, 29, 97)	80	6-31
	-120	(17, 18, 12)	16	0
GCHAZ-6s	-20	(233, 45, 156)	145	17-74
	-40	(45, 43, 72)	53	17-23
	-60	(20, 20, 12)	17	4
	-80	(7, 18, 7)	11	2
GCHAZ-10s	-5	(57, 232, 236)	175	17-75
	-20	(114, 80,34)	76	-
	-40	(17, 15, 35)	22	0-6
	-60	(30, 13, 34)	26	0-6
ICR-GCHAZ-12s	23	(202, 269, 214)	228	75-85
	-5	(225, 57,242)	175	30-74
	-20	(52, 51, 41)	48	21
	-60	(16, 16, 16)	16	6
NTR-ICR-GCHAZ-12s	23	(280, 290, 287)	286	100
	-5	(235, 202,247)	228	83
	-20	(87, 84, 93)	88	43
	-60	(25, 46, 40)	37	11-17

Table 7. Charpy impact toughness of X100-4 pipe steel and simulated HAZ regions

Region ID	Test Temperature, °C	Charpy Impact Energy, J	Average Charpy Impact Energy, J	Shear Area %
Pipe Steel BM	-20	(314, 319, 312)	315	100
	-60	(262, 309, 295)	289	100*
	-80	(248, 188, 252)	229	70-80*
	-100	(153, 173, 60)	129	21-59*
	-120	(159, 168, 11)	113	0-66*
GCHAZ-6s	-20	(237, 246, 278)	254	81-100
	-40	(206, 190, 241)	212	70-81
	-60	(35, 151, 114)	100	31-62
	-80	(20, 82, 33)	45	11-27
GCHAZ-10s	-5	(262, 265, 186)	238	74-85
	-20	(229, 273, 261)	254	77-88
	-40	(233, 167, 212)	204	65-79
	-60	(98, 78, 32)	69	17-33
	-80	(33, 47, 14)	31	0-17
ICR-GCHAZ-12s	-20	(248, 232, 222)	234	78-82
	-30	(192, 182, 210)	195	60-70
	-40	(94, 143, 96)	111	36-47
	-60	(27, 28, 58)	38	17-27

Note: *Splits were observed on fracture surfaces

Table 8. Charpy impact toughness of X80 pipe steel and simulated HAZ regions

Region ID	Test Temperature, °C	Charpy Impact Energy, J	Average Charpy Impact Energy, J	Average Shear Area %
Pipe Steel BM	-20	(312, 314, 282)	303	100*
	-40	(219, 204, 243)	222	~70**
	-50	(257, 26, 18)	100	21-85*
	-60	(23, 15, 200)	79	12-55**
	-80	(8, 6, 8)	7	0
GCHAZ-6s	23	(230, 65, 314)	203	40-100
	-5	(202, 232, 190)	208	60-71
	-20	(19, 40, 192)	84	0-55
	-60	(21, 11, 7)	13	0
ICR-GCHAZ-12s	23	(228, 241, 221)	230	75-81
	-5	(173, 150, 98)	140	33-63
	-20	(47, 46, 28)	40	12-17
	-60	(5, 11, 14)	10	0
NTR-ICR-GCHAZ-12s	23	(242, 233, 231)	235	78-82
	-5	(43, 48, 232)	108	23-70
	-20	(22, 32, 75)	45	6-27
	-60	(9, 15, 16)	13	0

Note: *Splits were observed on fracture surfaces. **Major splitting

Table 9. Summary of ETT and Charpy impact energies at -60°C and -20°C

Pipe	X100-2			X100-5			X100-4			X80		
Material Condition	ETT °C	Energy -60°C, J	Energy -20°C, J	ETT °C	Energy -60°C, J	Energy -20°C, J	ETT °C	Energy -60°C, J	Energy -20°C, J	ETT °C	Energy -60°C, J	Energy -20°C, J
Pipe Steel	-87	259	272	-70	237	287	-98	289	315	-46	79	303
GCHAZ-6s	-50	92	247	-25	17	145	-50	100	254	-18	13	84
GCHAZ-10s	-40	38	152	-7	26	76	-50	69	254	-	-	-
ICR-GCHAZ	-	-	-	-11	16	48	-40	38	234	-6	10	40
NTR-ICR-GCHAZ	-	-	-	-12	37	88	-	-	-	-4	13	45

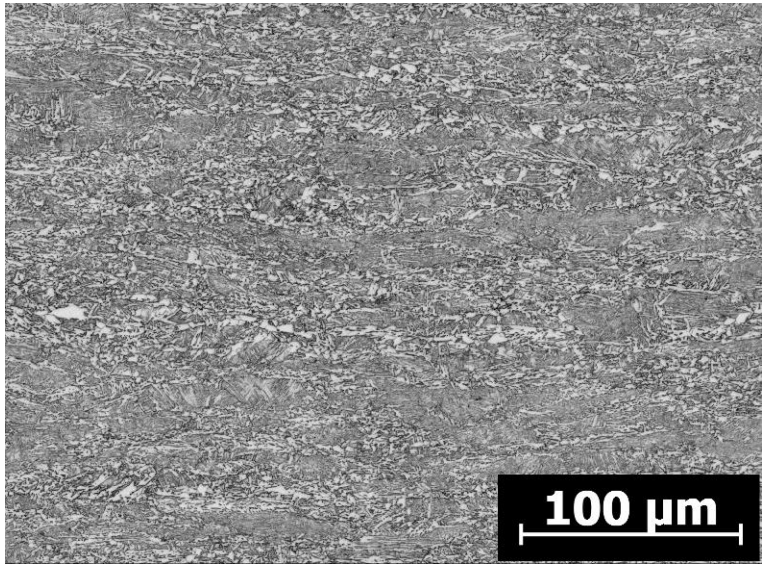

(a)

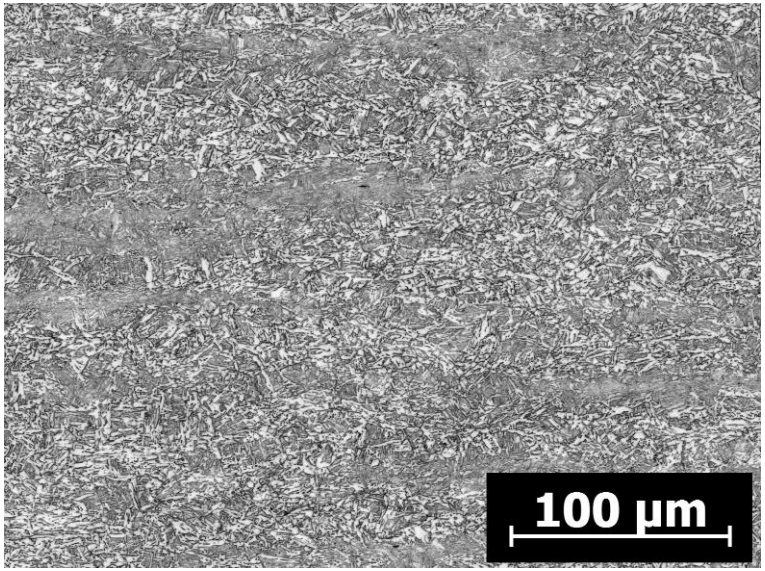

(b)

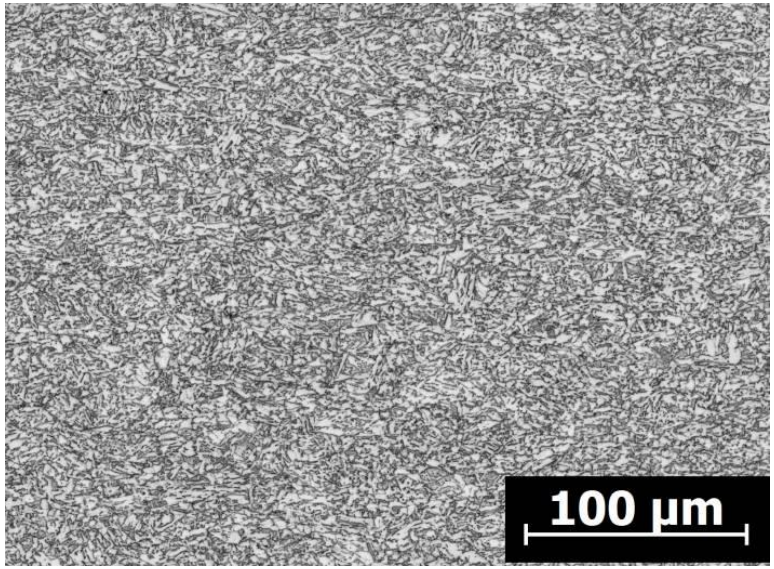

(c)

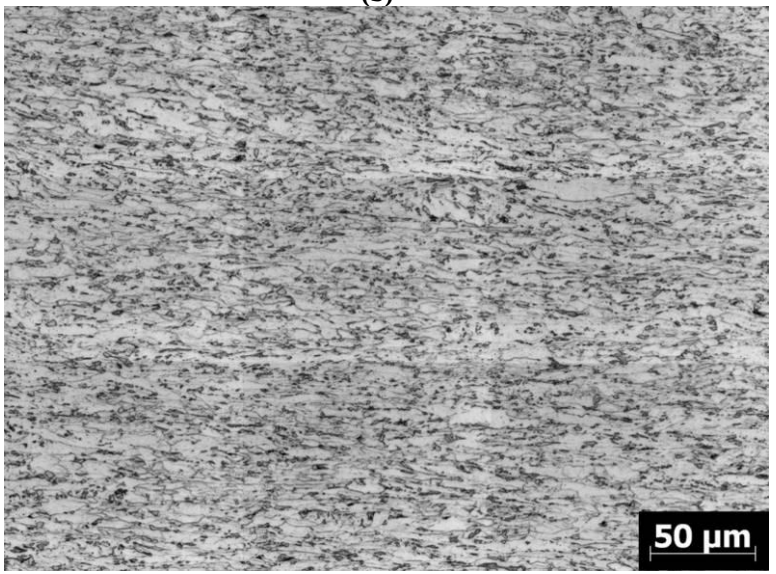

(d)

Figure 1. Microstructure of the pipe materials (a) X100-2 (b) X100-5 (c) X100-4 and (d) X80

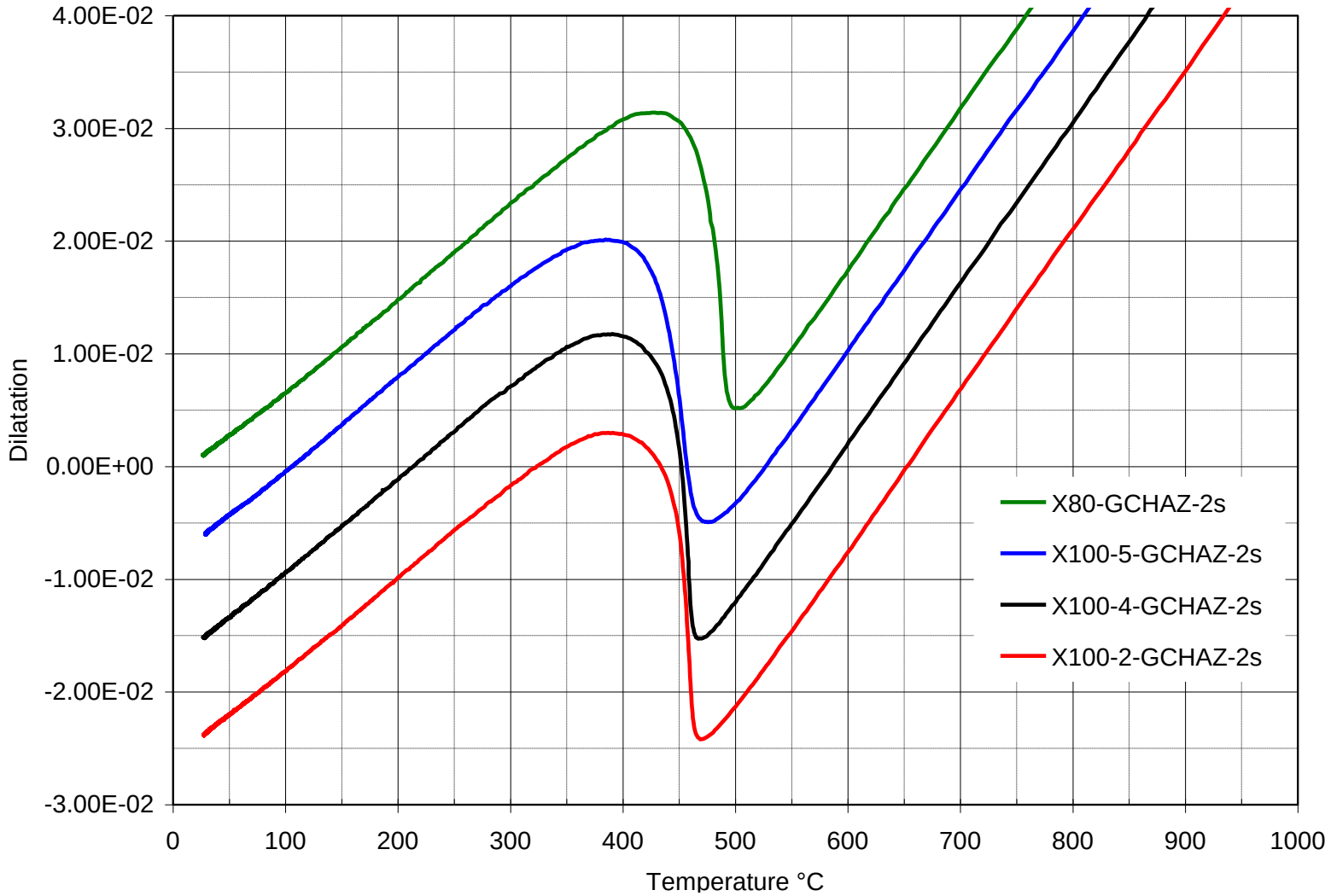

Figure 2. Dilatation curves for simulated GCHAZ for Tp= 1350°C with a 1 s hold and cooling time $\Delta t_{800\text{-}500}$ ~2 s.

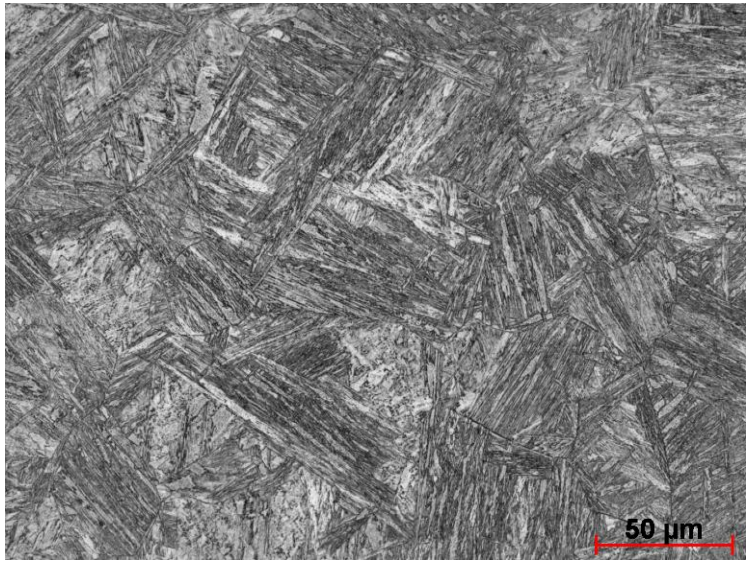

(a) X100-2 with $\Delta t_{800\text{-}500}$ = 1.8 s: 360 HV (347-378)

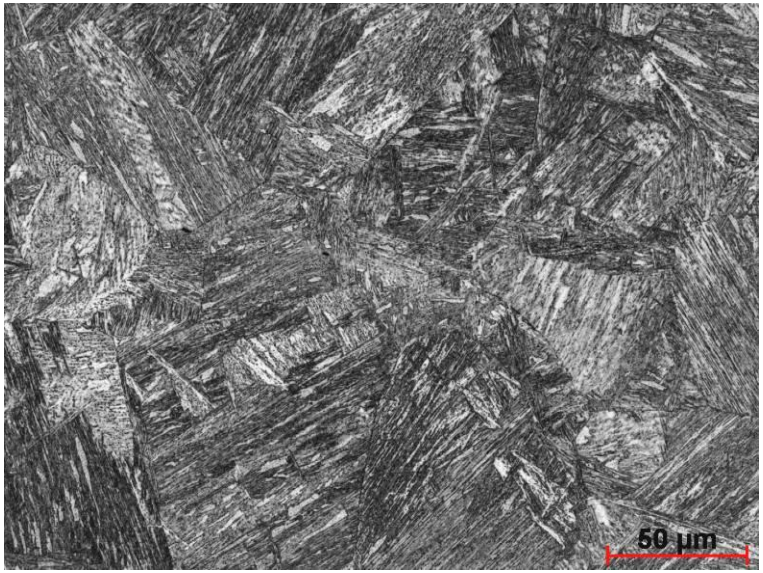

(b) X100-5 with $\Delta t_{800\text{-}500}$ = 1.9 s: 344 HV (311-363)

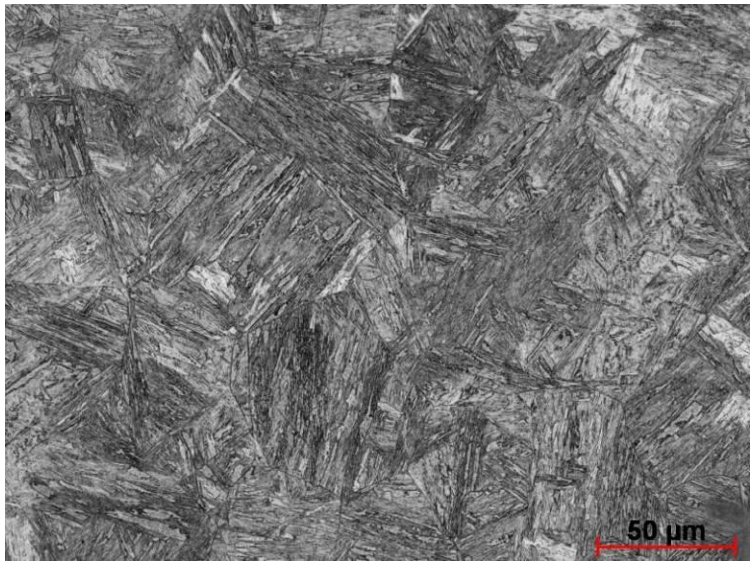

(c) X100-4 with $\Delta t_{800\text{-}500}$ = 2.0 s: 336 HV (326-344)

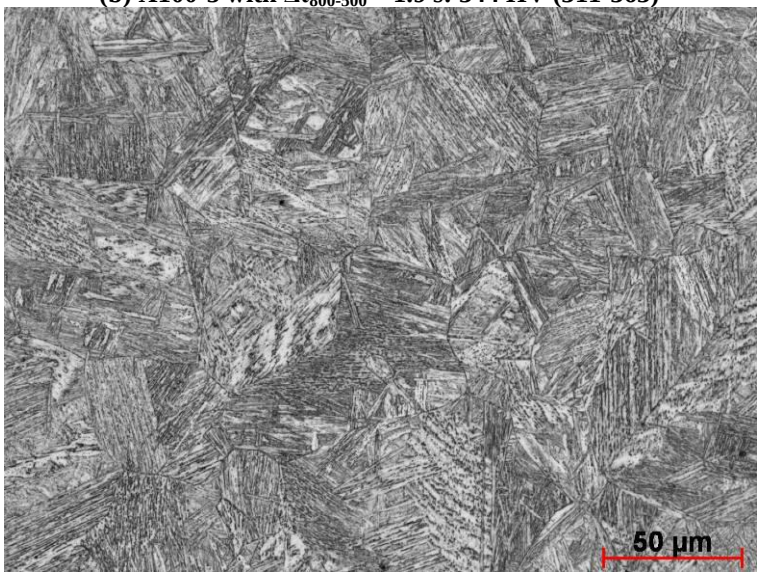

(d) X80 with $\Delta t_{800\text{-}500}$ = 1.8 s: 319 HV (310-329)

Figure 3. Microstructures of simulated GCHAZ with cooling time Δt800-500 ~2 s.

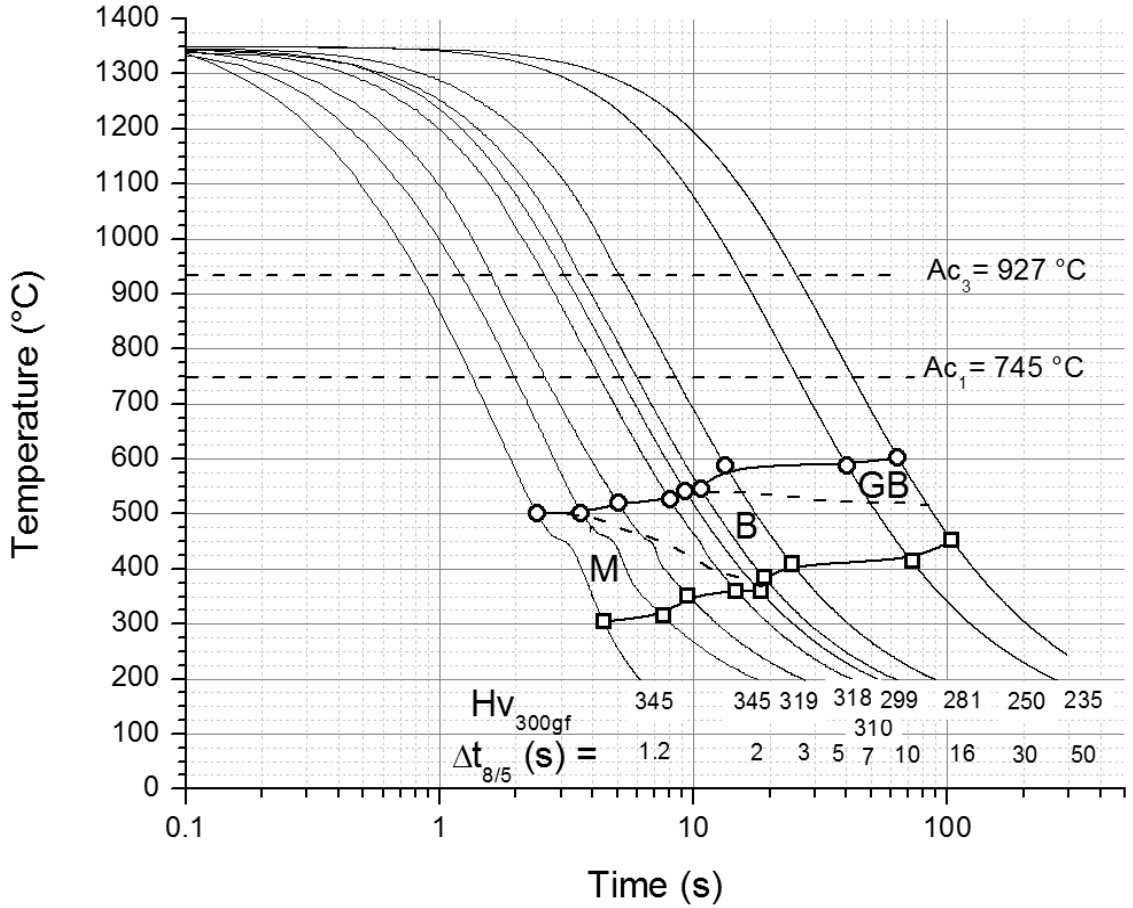

Figure 4. CCT diagram for X100-2 from 1350 °C showing the formation of martensite (M), bainite (B) and granular bainite (GB)

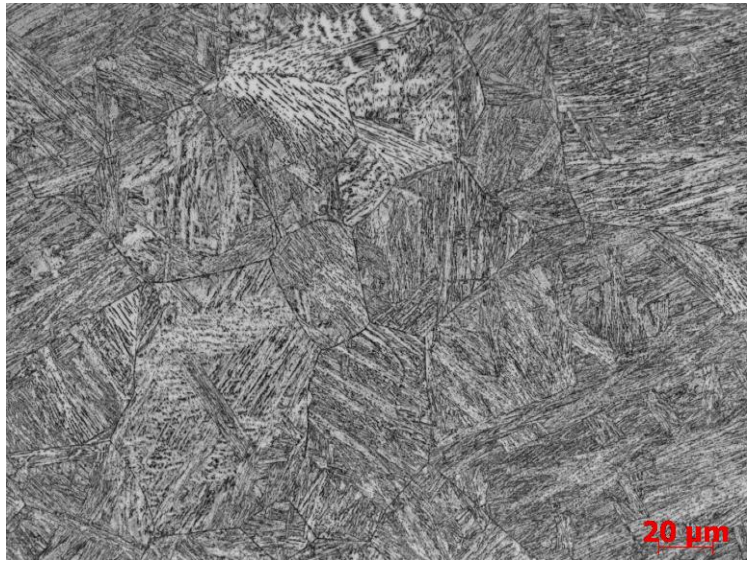

(a) $\Delta t_{800\text{-}500}$ = 6 s

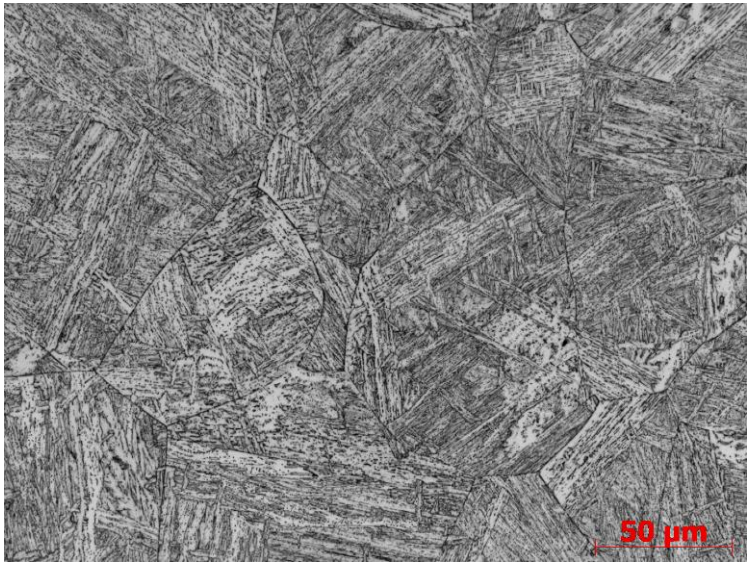

(b) $\Delta t_{800\text{-}500}$ = 10 s

(c) $\Delta t_{800\text{-}500}$ = 30 s

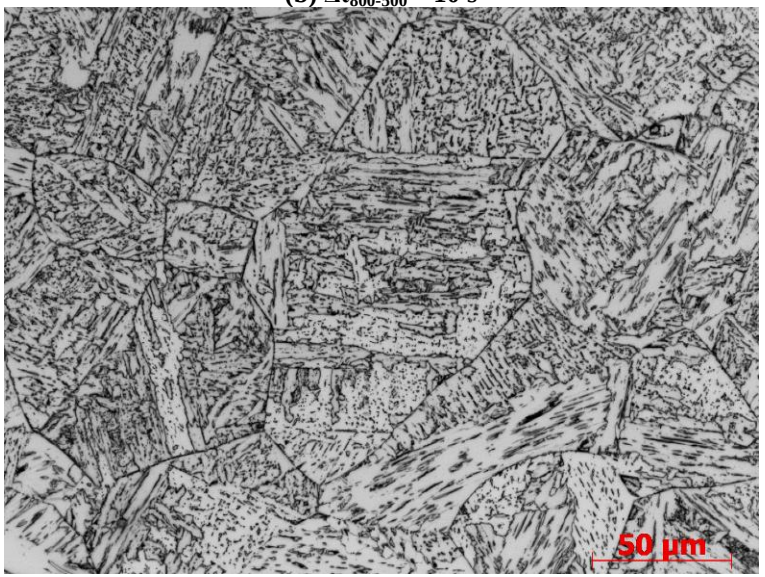

(d) $\Delta t_{800\text{-}500}$ = 50 s

Figure 5. Microstructure evolution of simulated GCHAZ for X100-2 pipe steel.

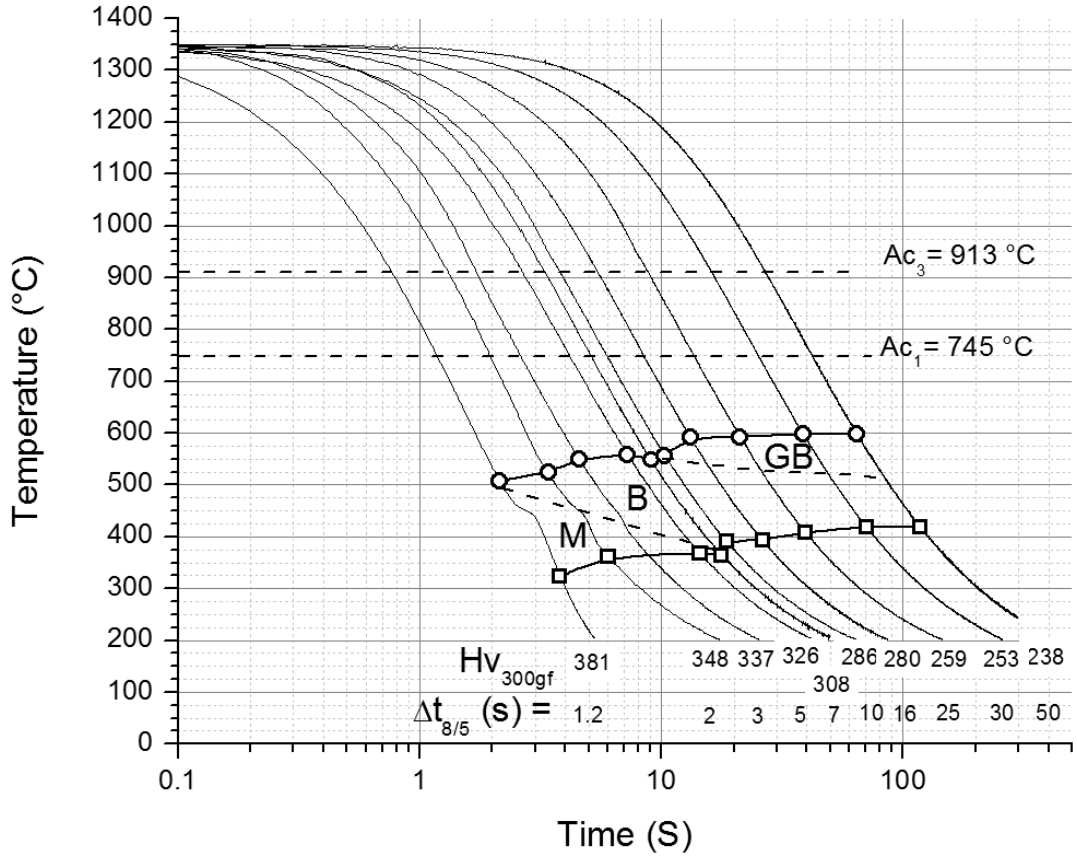

Figure 6. CCT diagram for X100-5 from 1350 °C showing the formation of martensite (M), bainite (B) and granular bainite (GB)

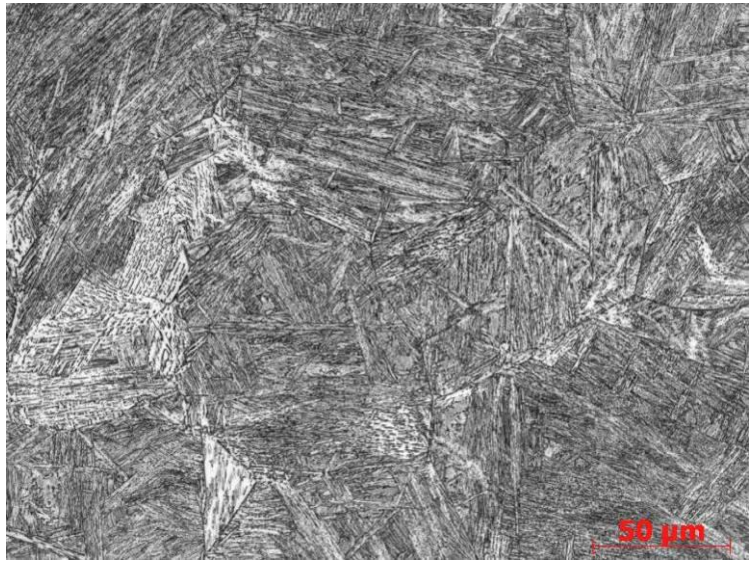

(a) $\Delta t_{800\text{-}500}$ = 6 s

(b) $\Delta t_{800\text{-}500}$ = 10 s

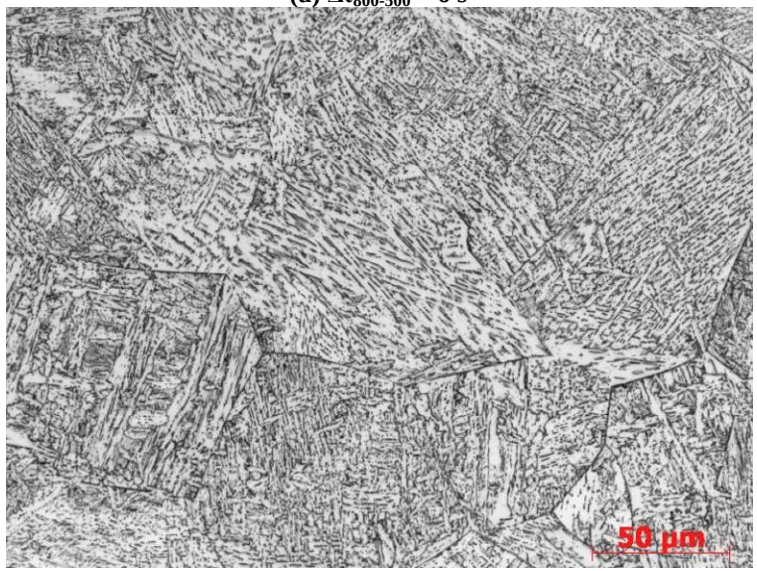

(c) $\Delta t_{800\text{-}500}$ = 30 s

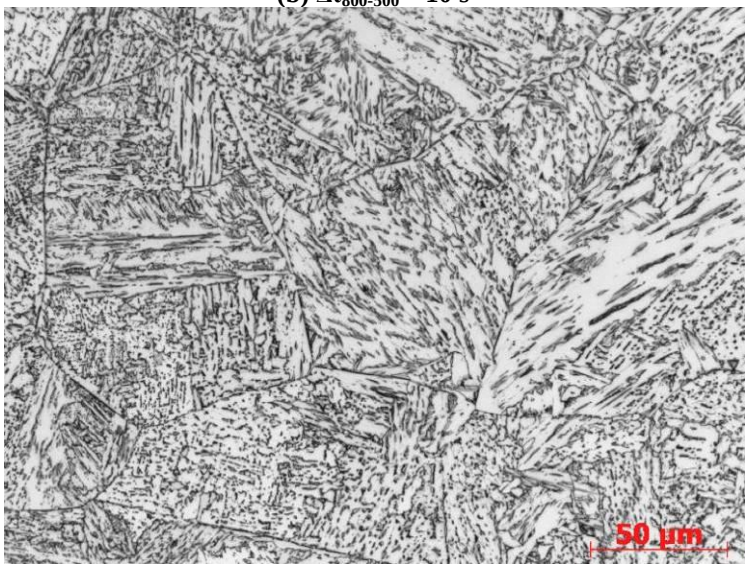

(d) $\Delta t_{800\text{-}500}$ = 50 s

Figure 7. Microstructure evolution of simulated GCHAZ for X100-5 pipe steel.

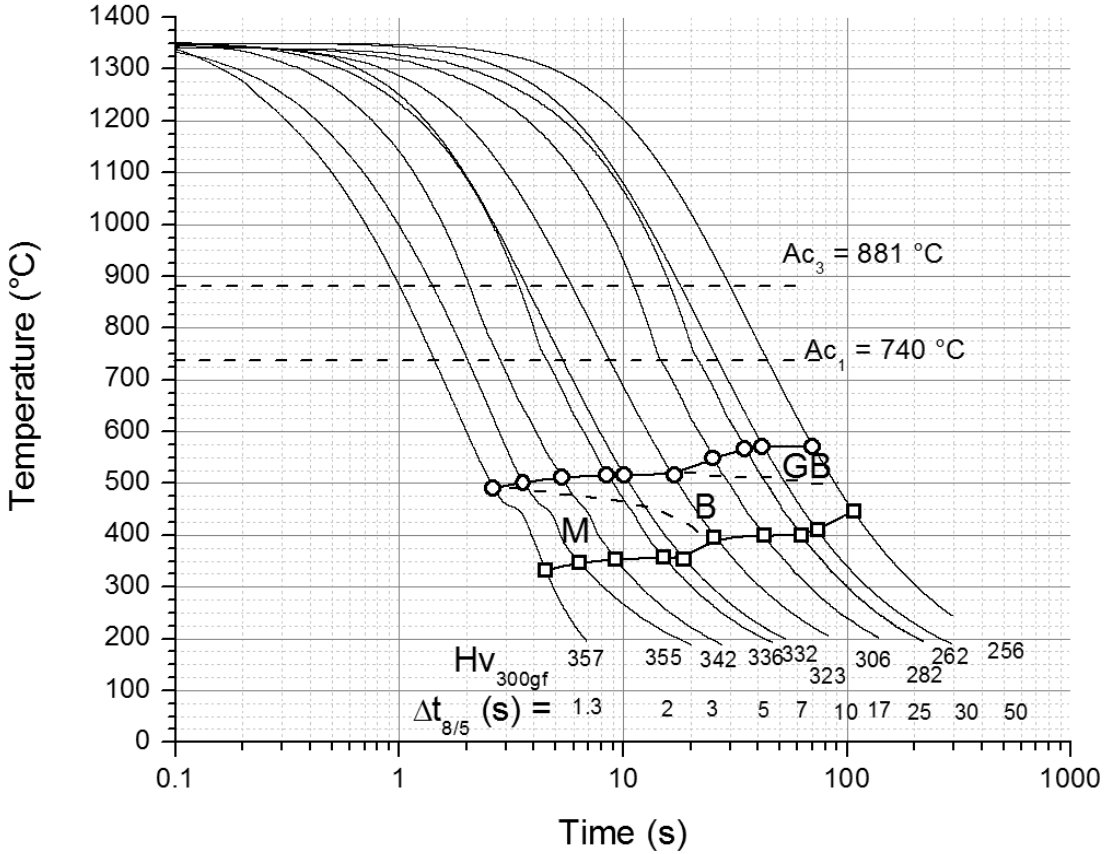

Figure 8. CCT diagram for X100-4 from 1350 °C showing the formation of martensite (M), bainite (B) and granular bainite (GB)

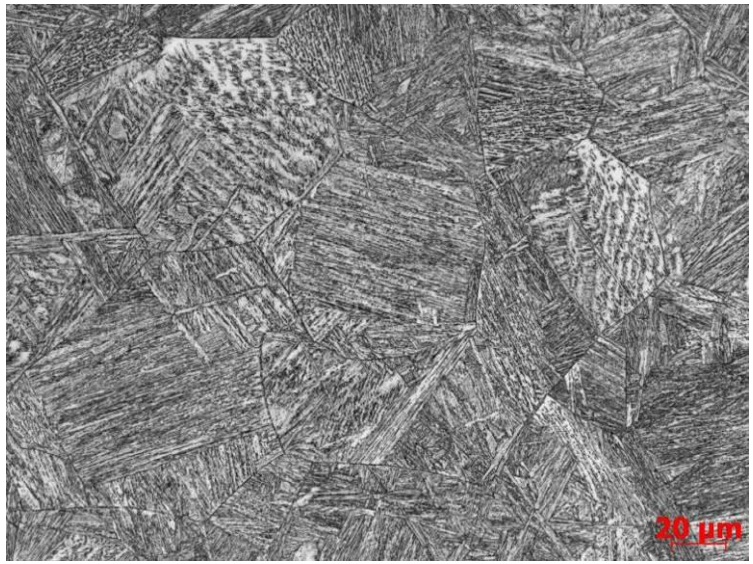

(a) $\Delta t_{800\text{-}500}$ = 6 s

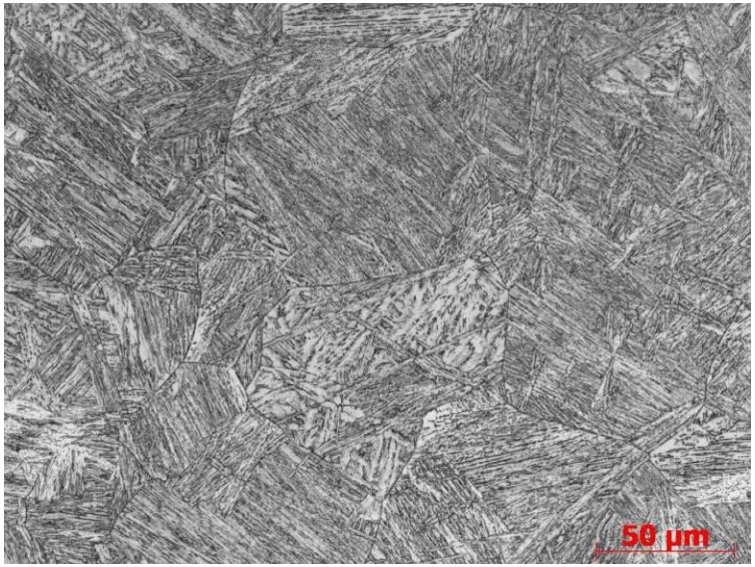

(b) $\Delta t_{800\text{-}500}$ = 10 s

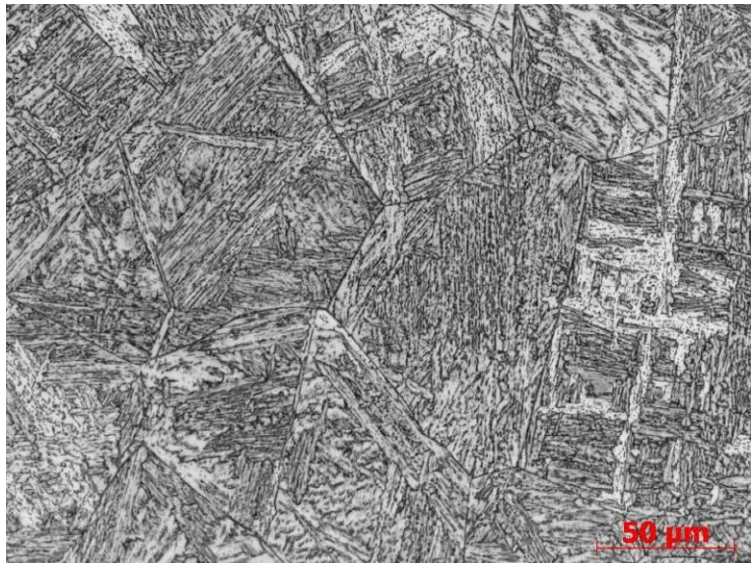

(c) $\Delta t_{800\text{-}500}$ = 30 s

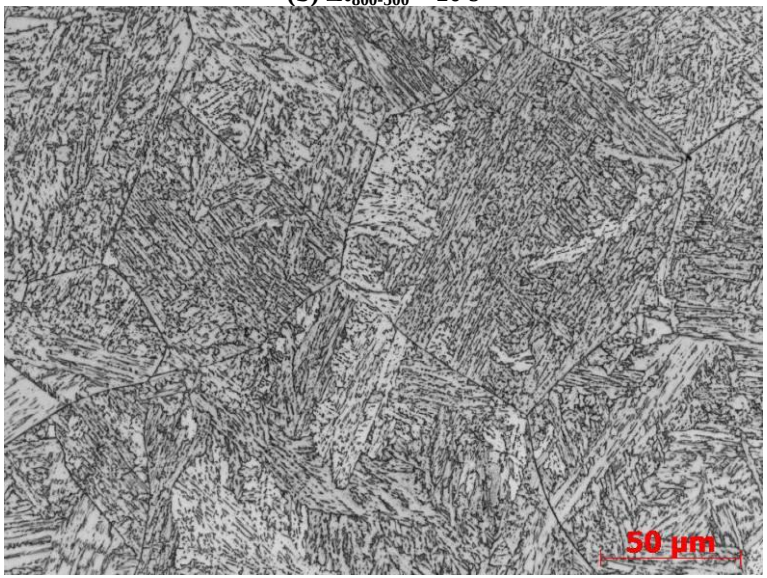

(d) $\Delta t_{800\text{-}500}$ = 50 s

Figure 9. Microstructure evolution of simulated GCHAZ for X100-4 pipe steel.

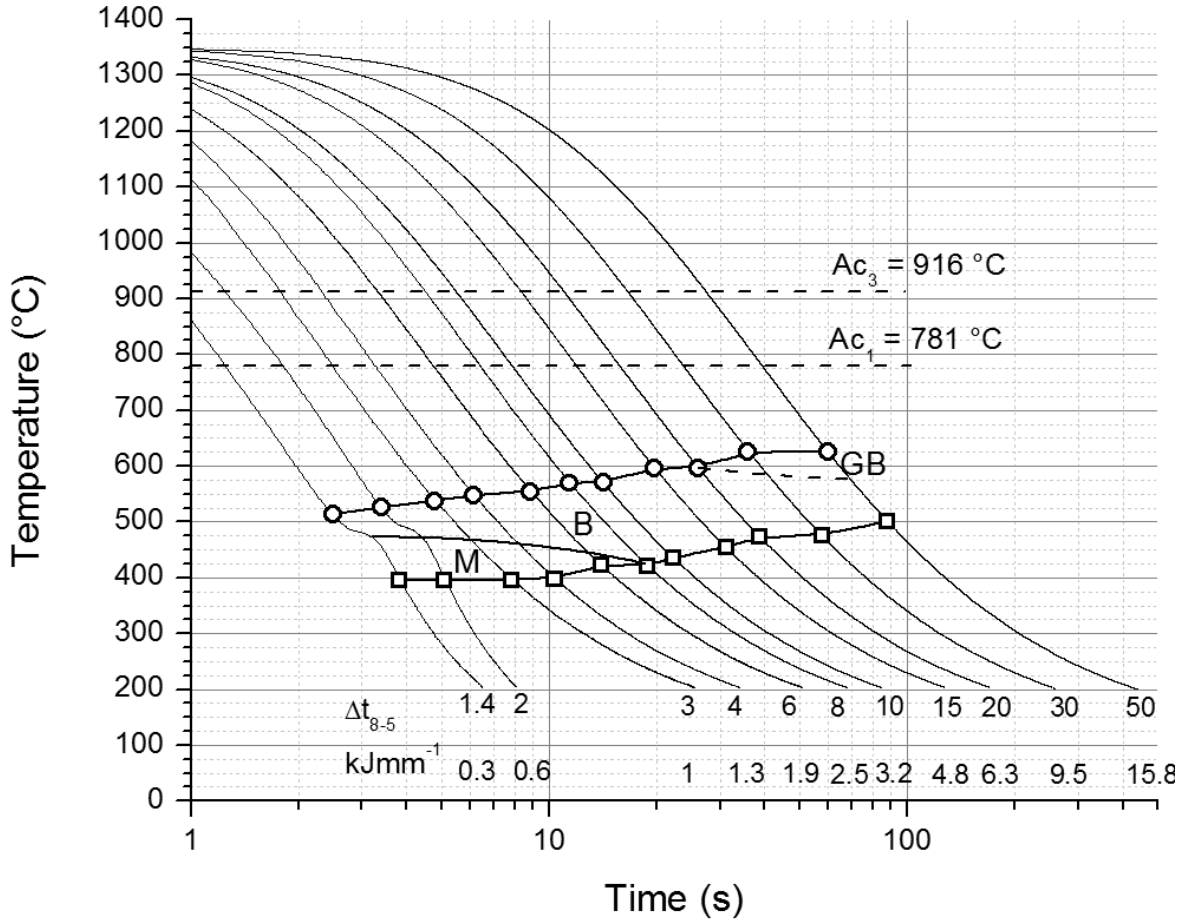

Figure 10. CCT Diagram for X80 from 1350 °C showing the formation of martensite (M), bainite (B) and granular bainite (GB)

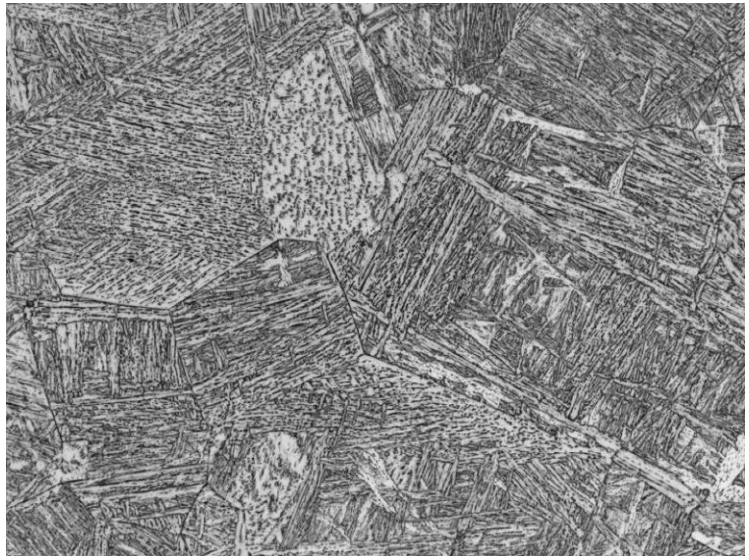

(a) $\Delta t_{800-500}$ = 6 s

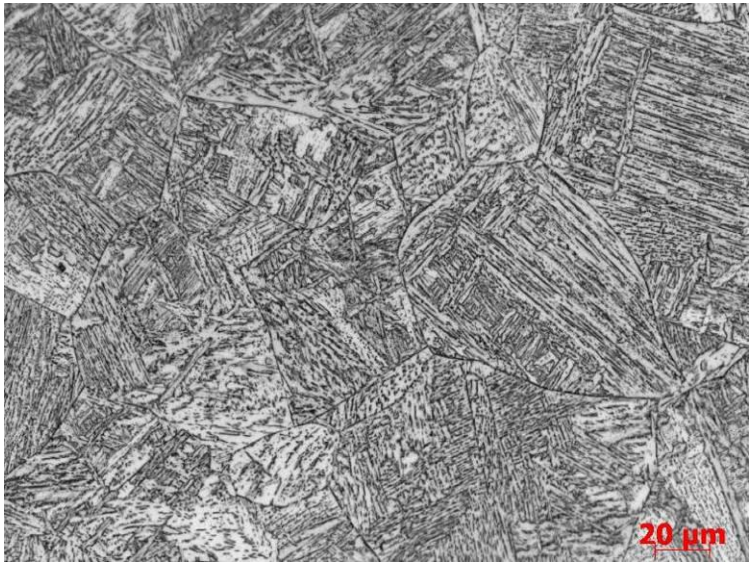

(b) $\Delta t_{800-500}$ = 10 s

(c) $\Delta t_{800-500}$ = 30 s

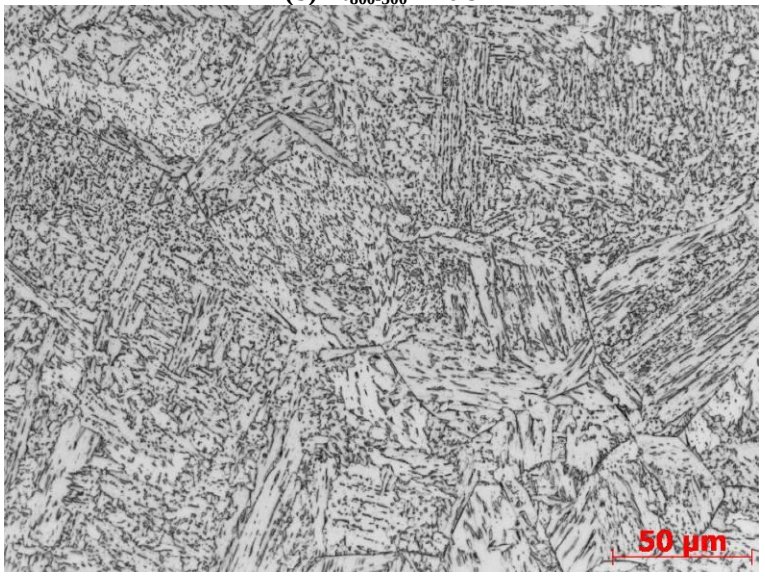

(d) $\Delta t_{800-500}$ = 50 s

Figure 11. Microstructure evolution of simulated GCHAZ for X80 pipe steel.

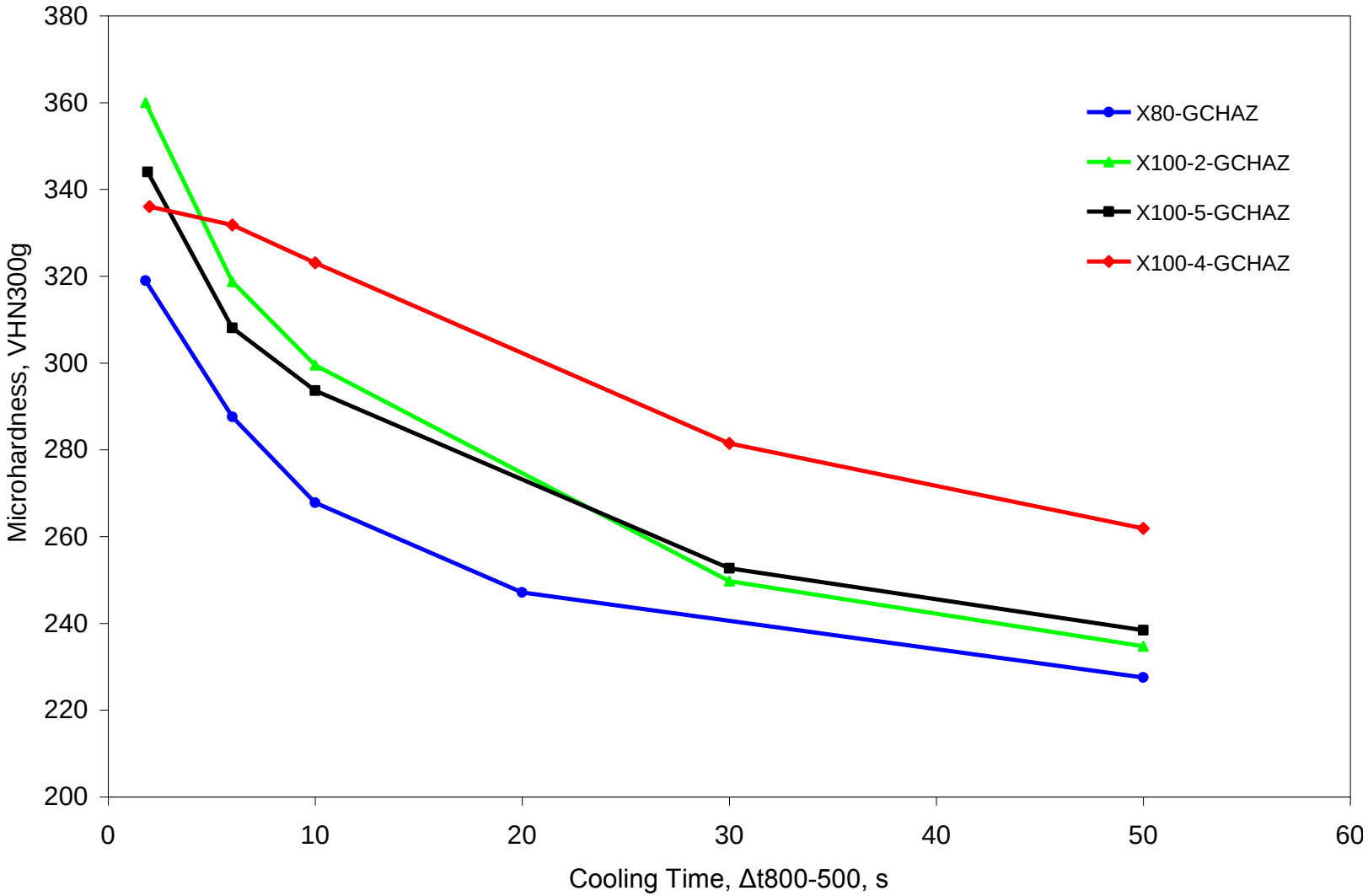

Figure 12. Average microhardness as a function of cooling time ($\Delta t_{800\text{-}500}$) for simulated GCHAZ regions in X100 and X80 pipe steels.

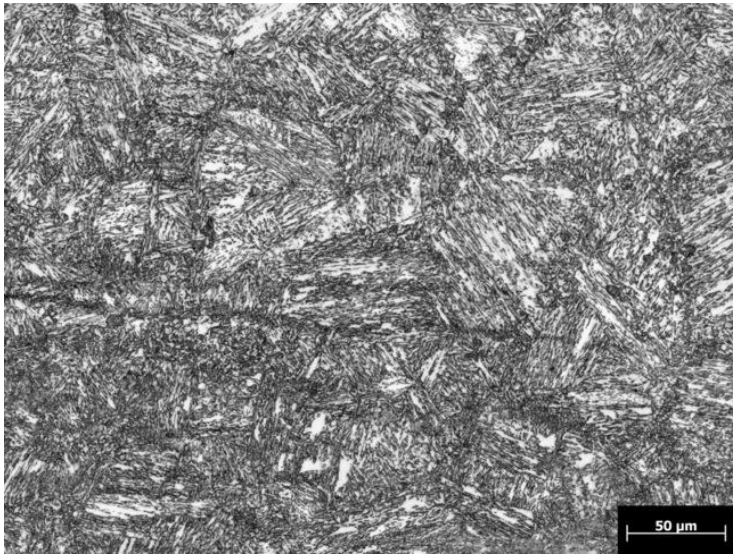

(a)

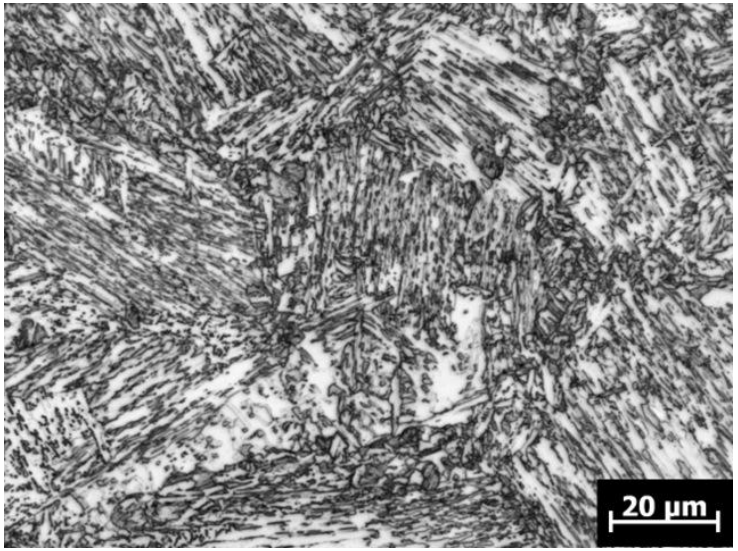

(b)

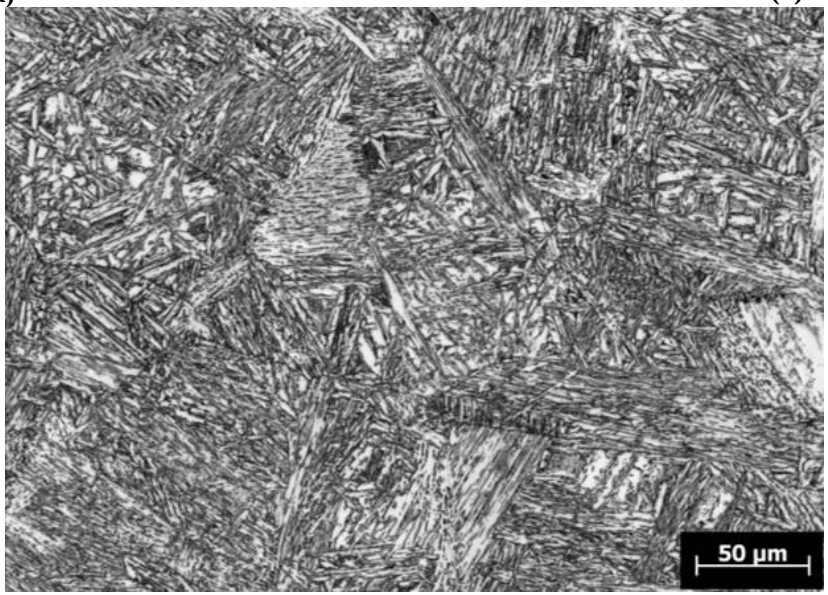

(c)

Figure 13. Optical micrographs of simulated (a, b) ICRGCHAZ and (c) NTR-ICRGCHAZ for X100-5 pipe steel.

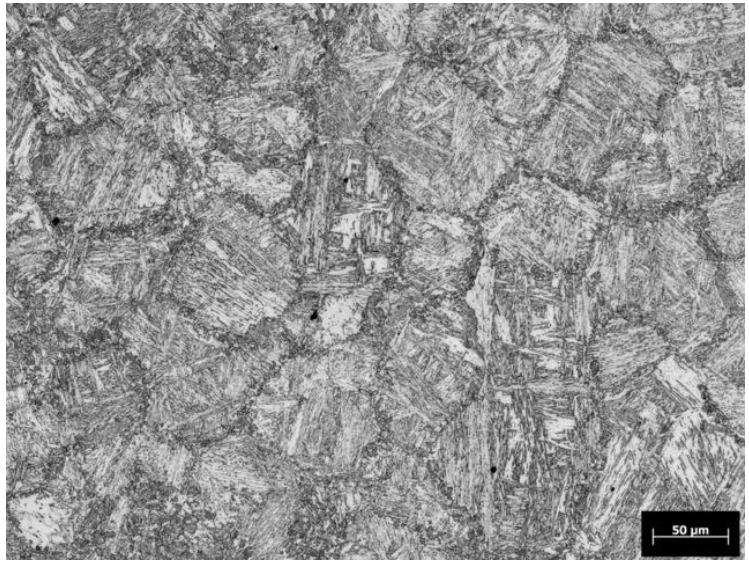

(a)

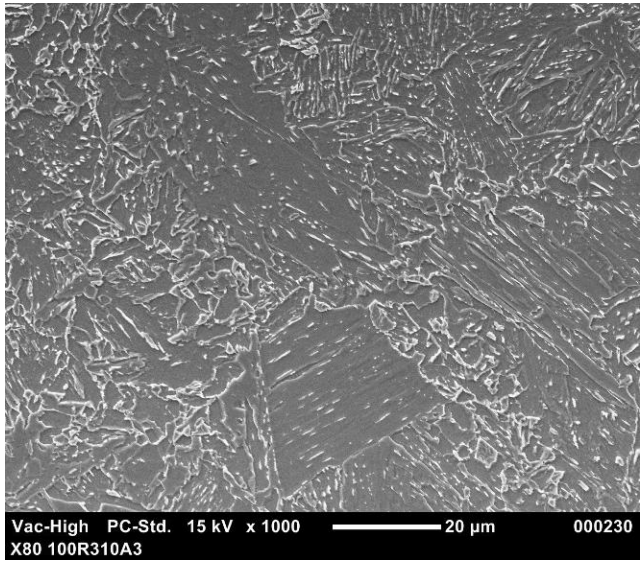

(b)

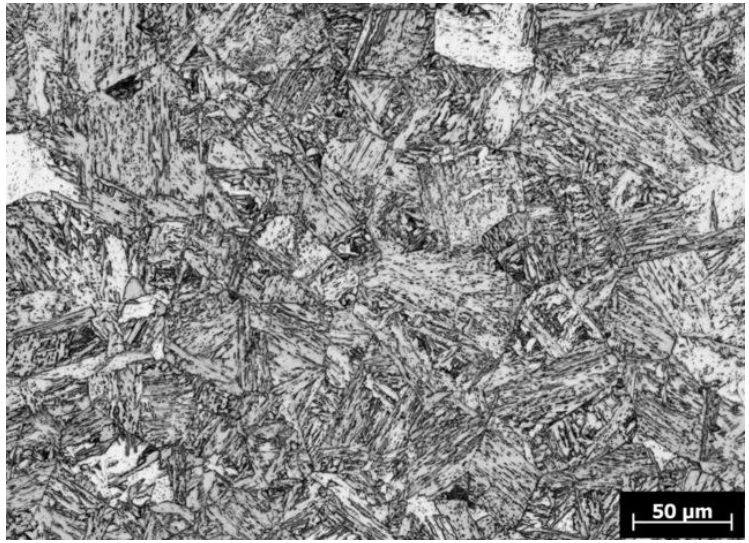

(c)

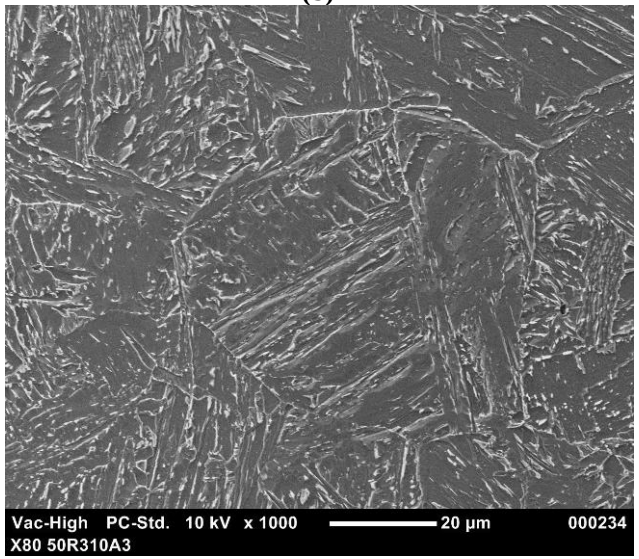

(d)

Figure 14. Optical and SEM micrographs of the simulated (a, b) ICR-GCHAZ and (c, d) NTR-ICRGCHAZ for X80 pipe steel.

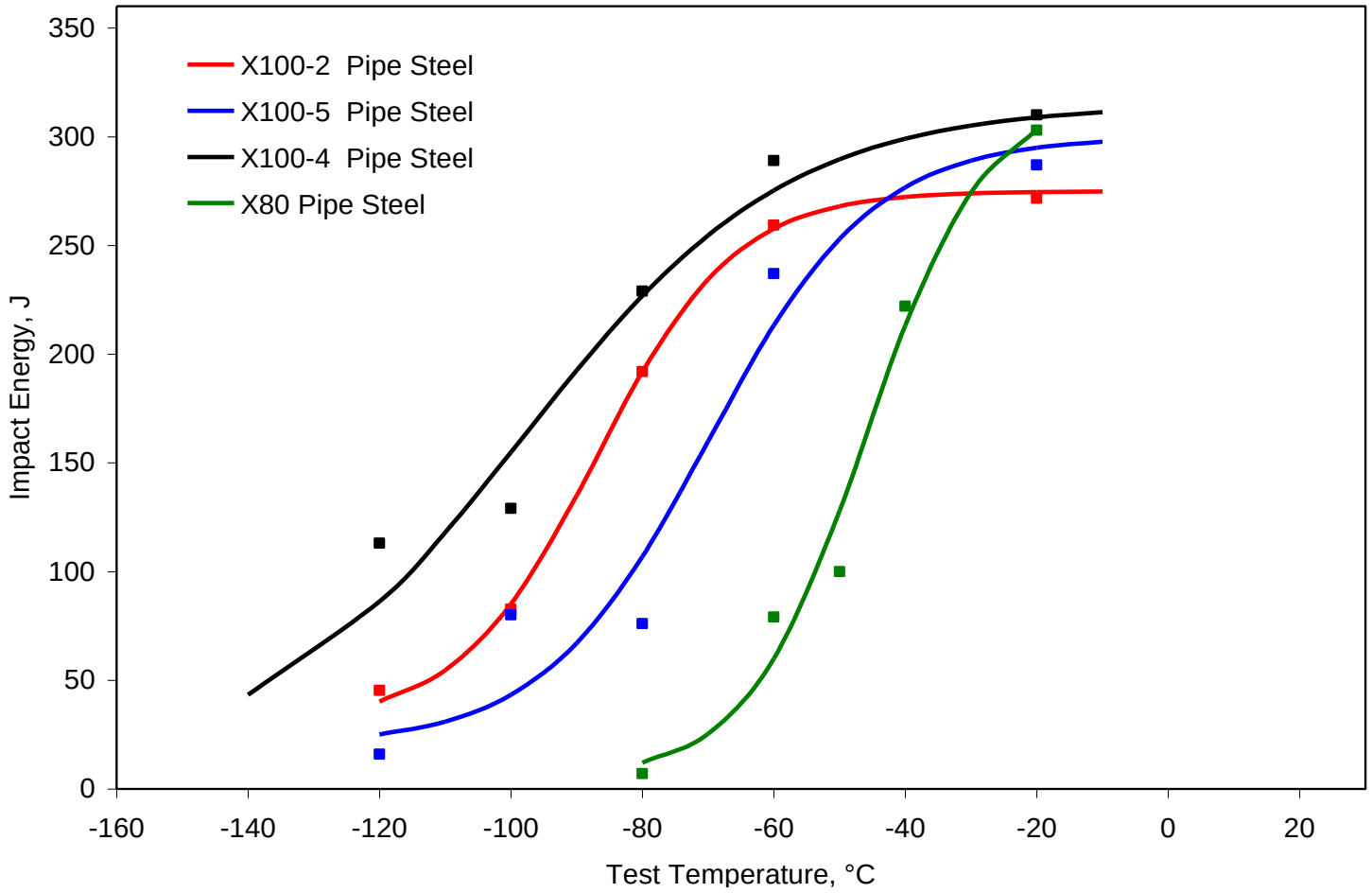

Figure 15. Charpy transition curves for X100 and X80 pipe steels.

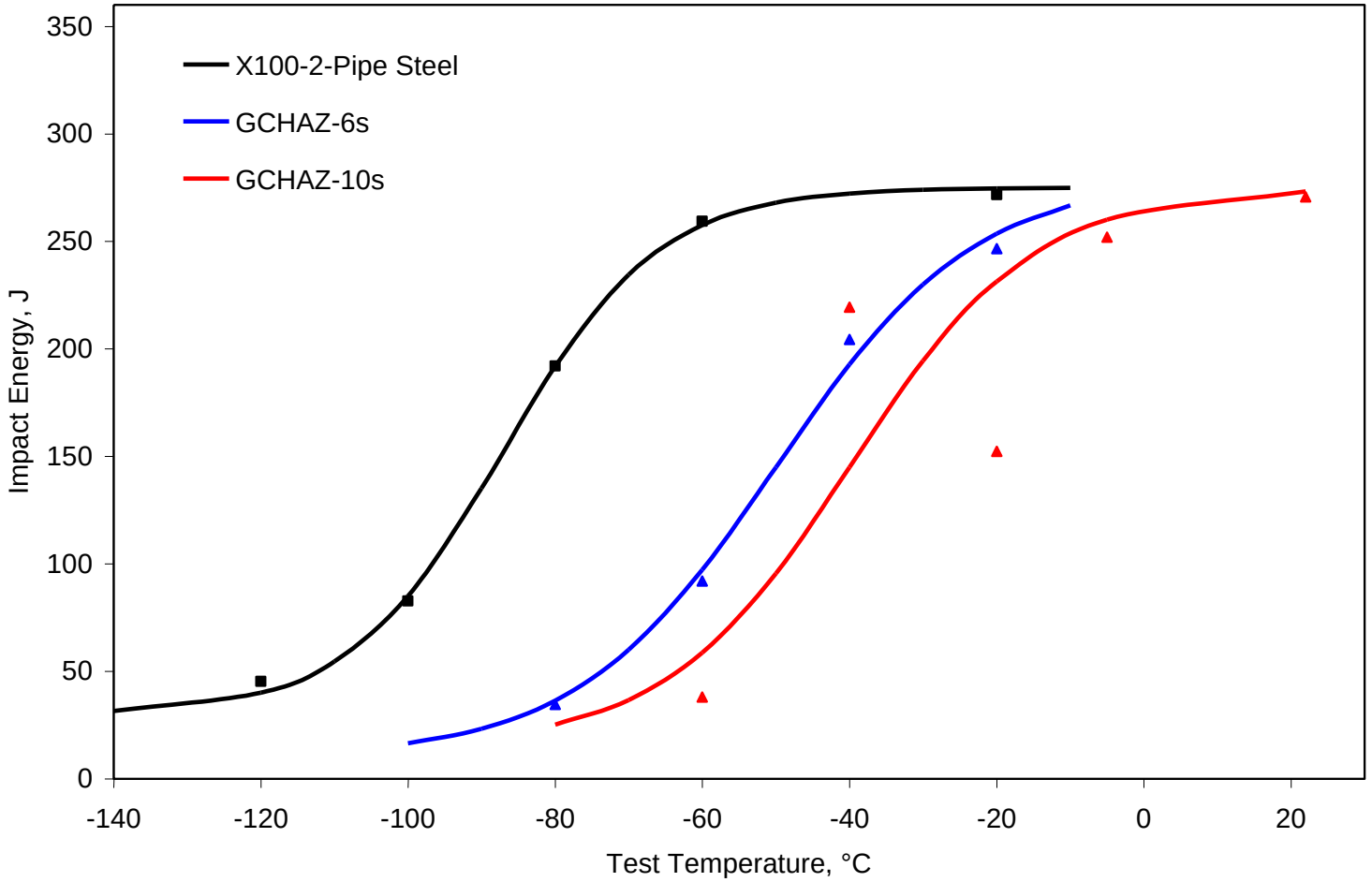

Figure 16. Charpy transition curves for X100-2 pipe steel and simulated GCHAZ regions.

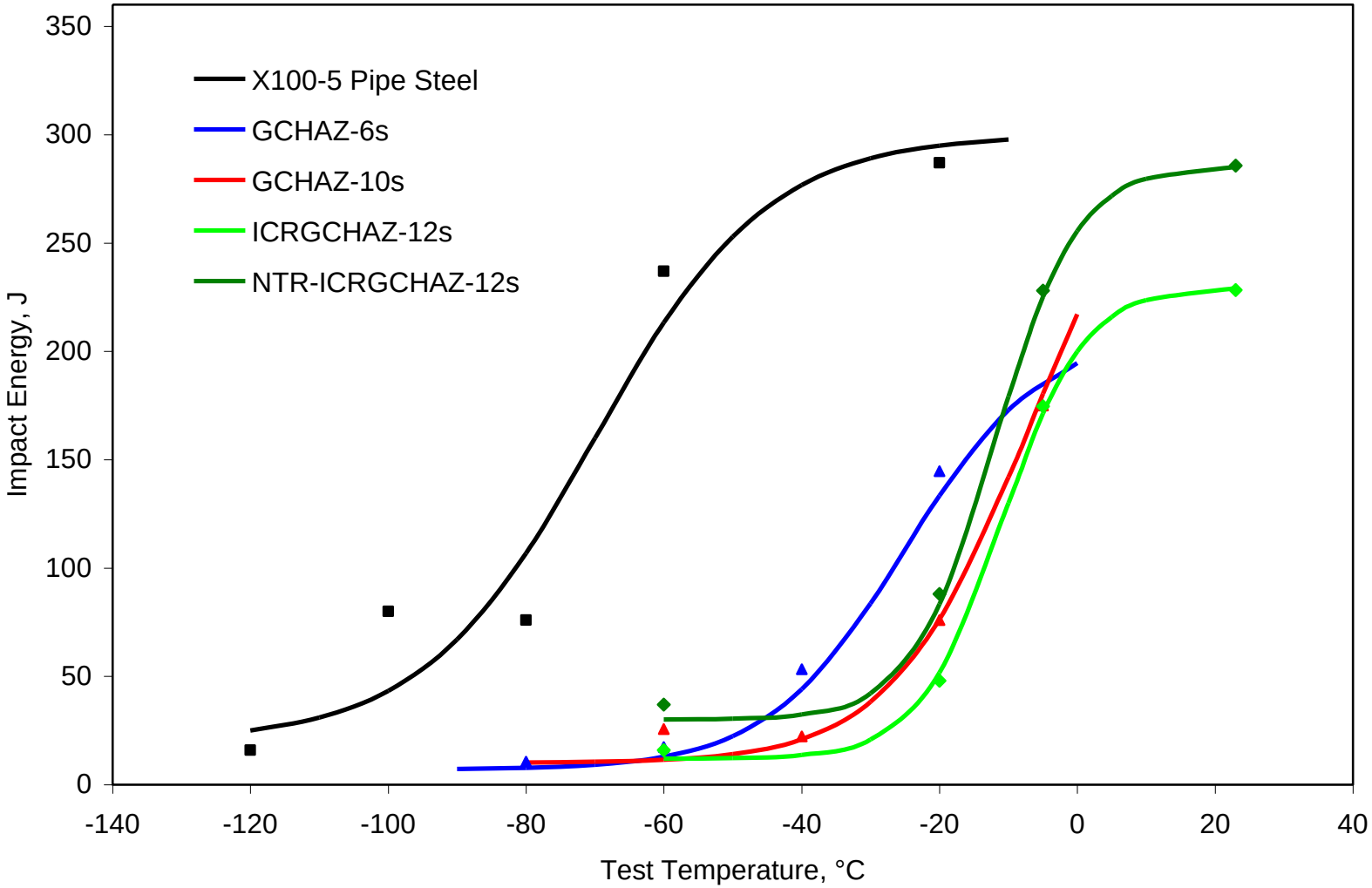

Figure 17. Charpy transition curves for X100-5 pipe steel and simulated HAZ regions.

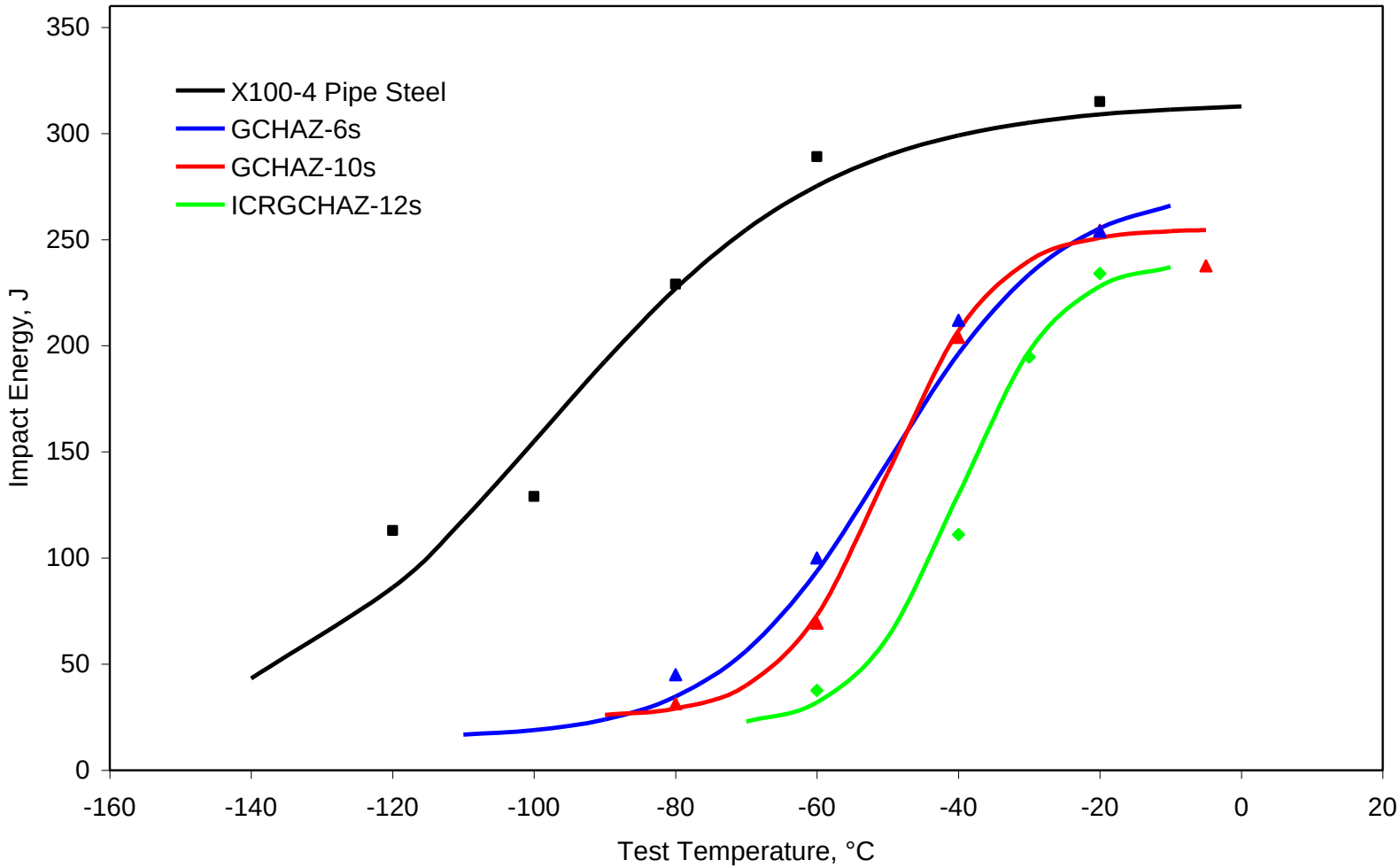

Figure 18. Charpy transition curves for X100-4 pipe steel and simulated HAZ regions.

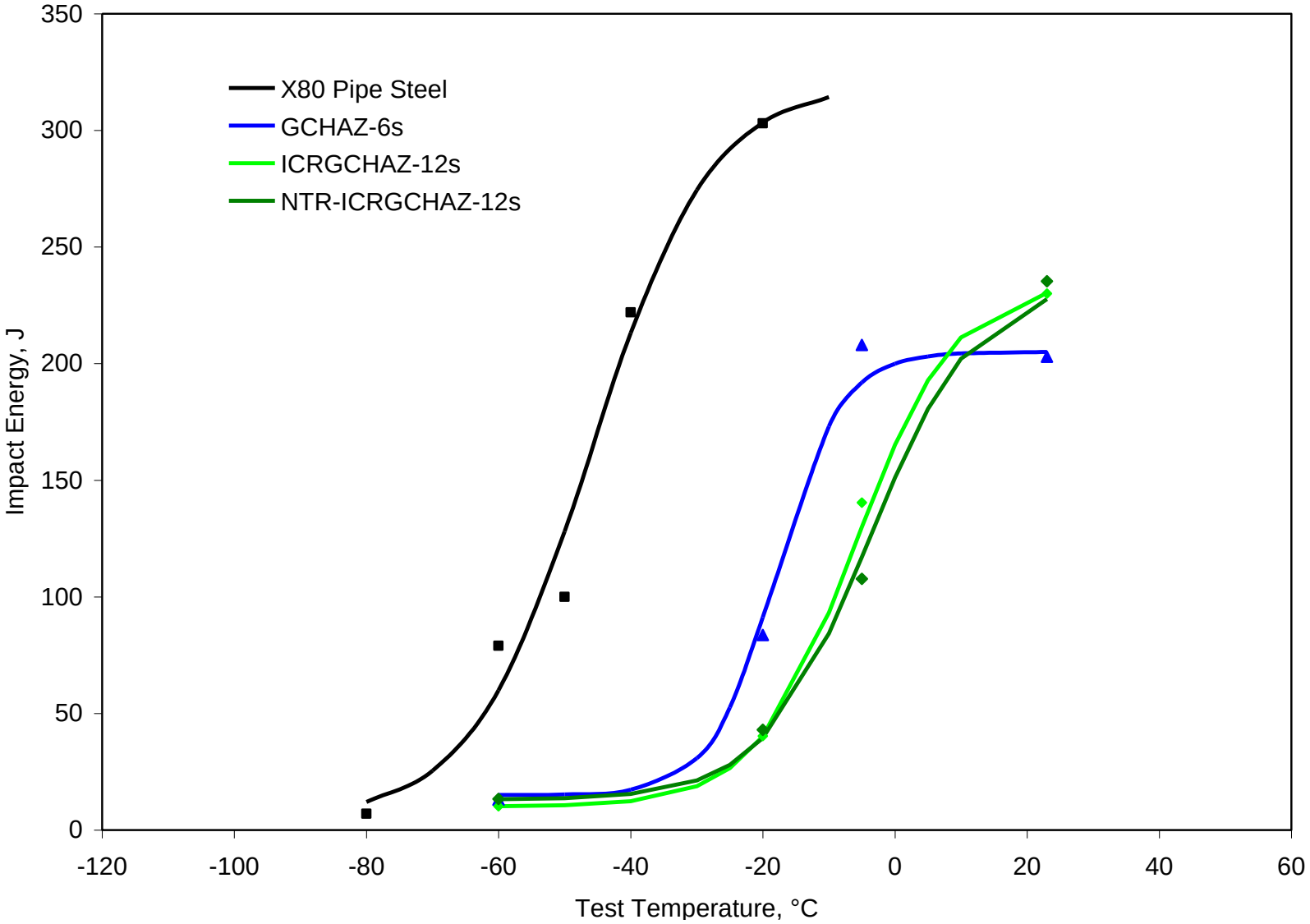

Figure 19. Charpy transition curves for X80 pipe steel and simulated HAZ regions.

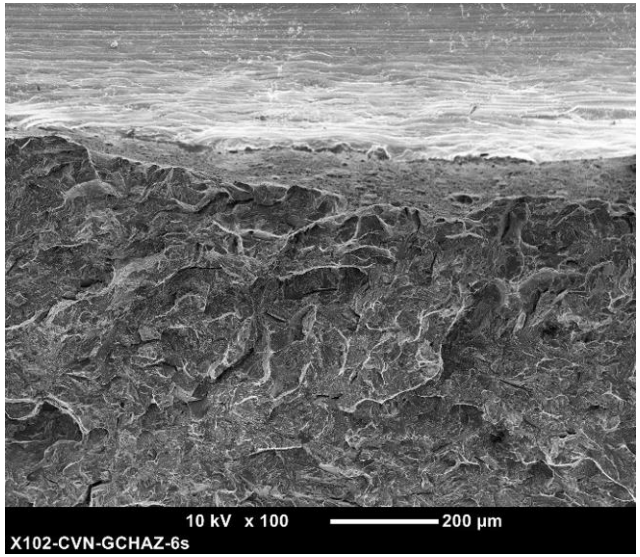

(a)

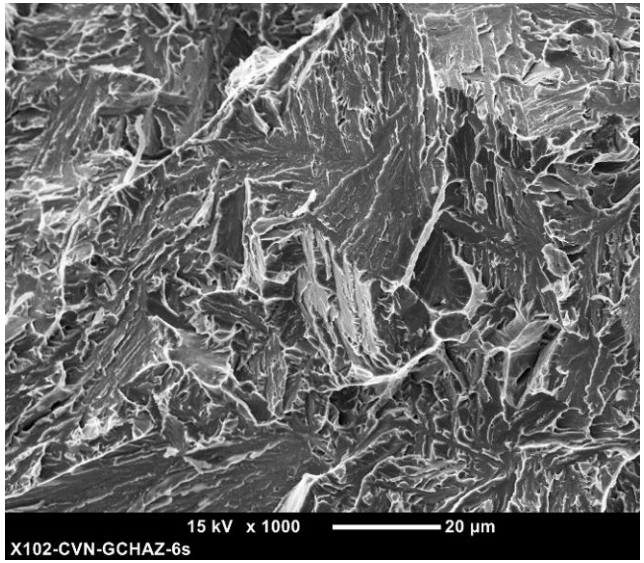

(b)

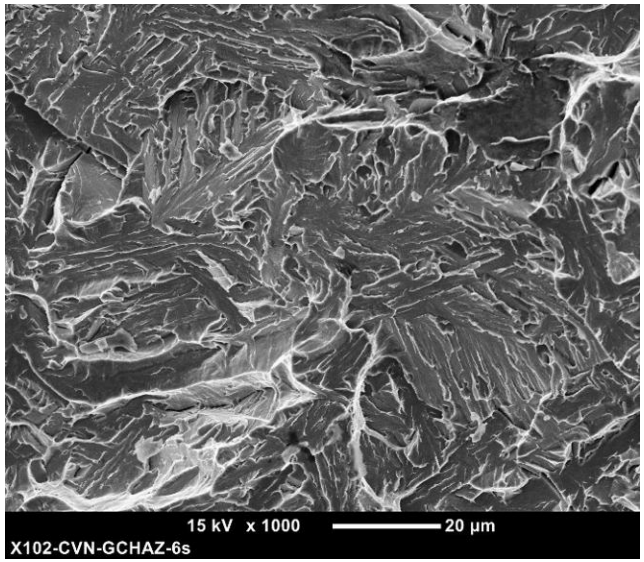

(c)

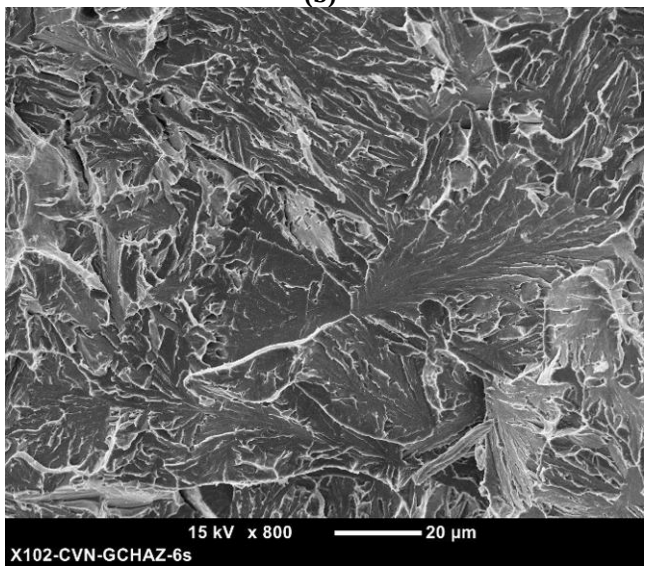

(d)

Figure 20. Fractographs showing detail of fracture surface of X100-2 CVN-GCHAZ $\Delta t_{800\text{-}500}$ = 6 s specimen, 16 J at –80°C.

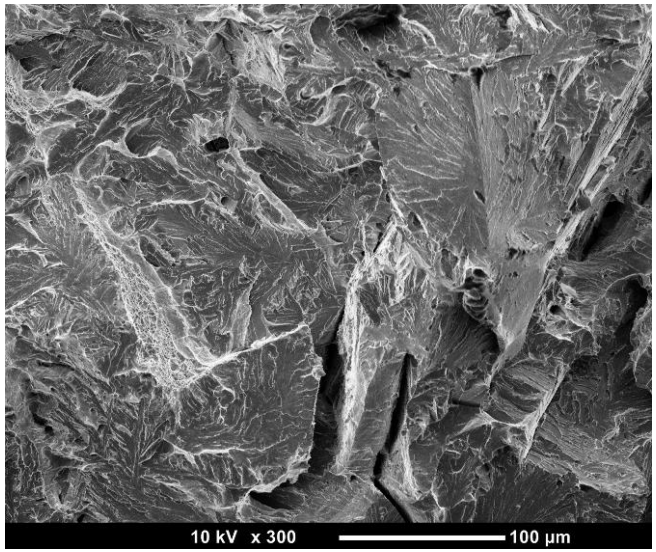

(a)

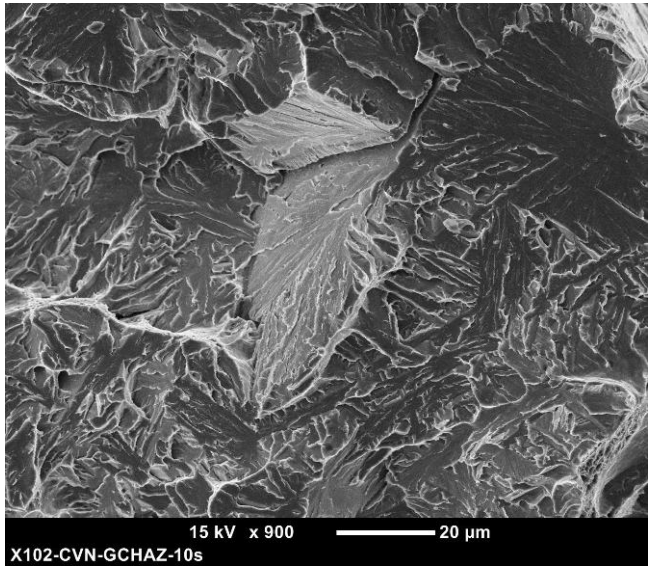

(b)

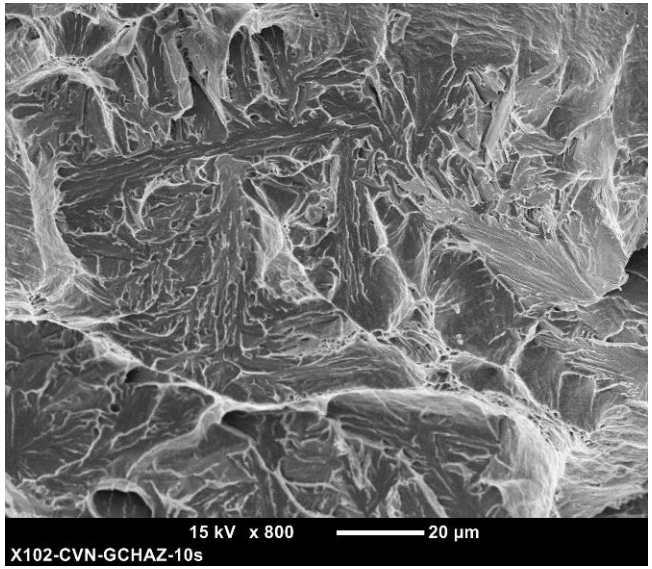

(c)

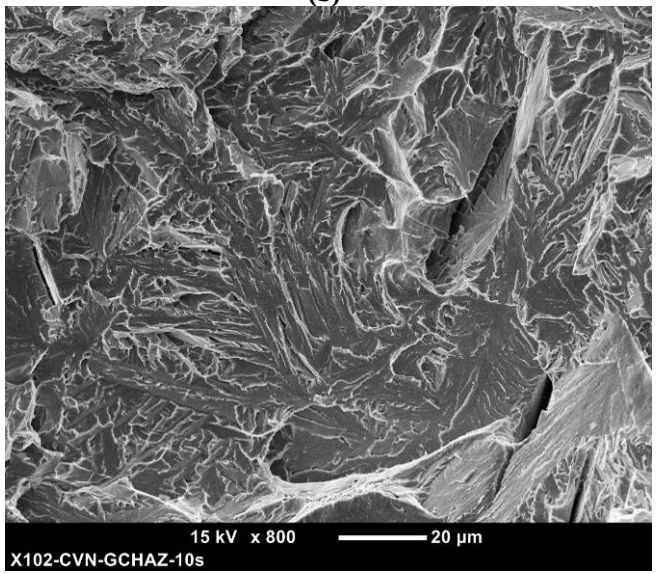

(d)

Figure 21. Fractographs showing detail of fracture surface of X100-2 CVN-GCHAZ $\Delta t_{800\text{-}500}$ = 10 s specimen, 30 J at –60°C.

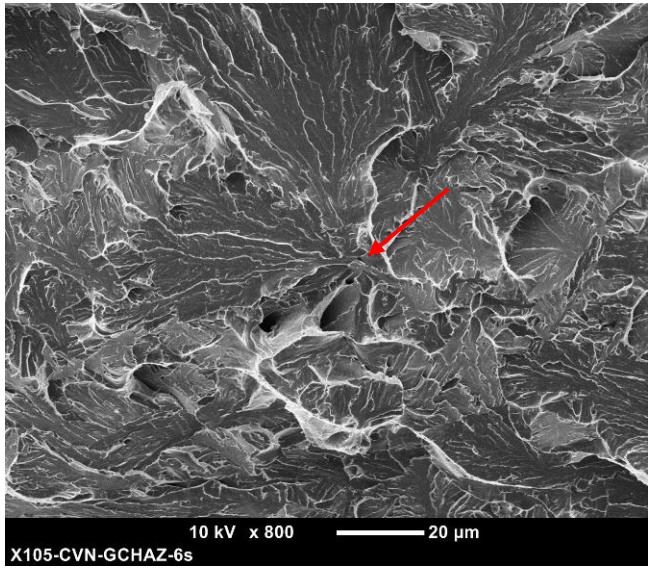

(a)

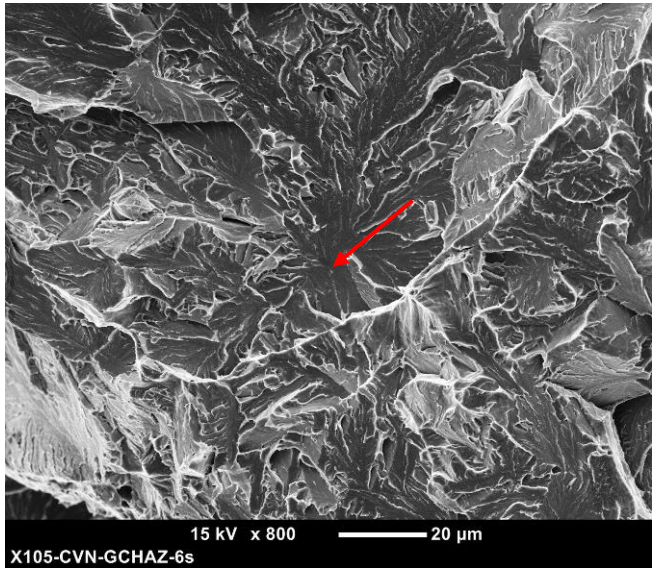

(b)

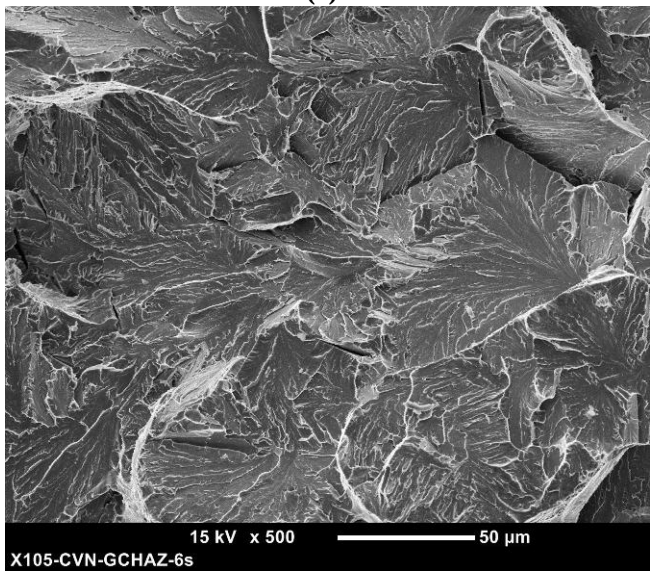

(c)

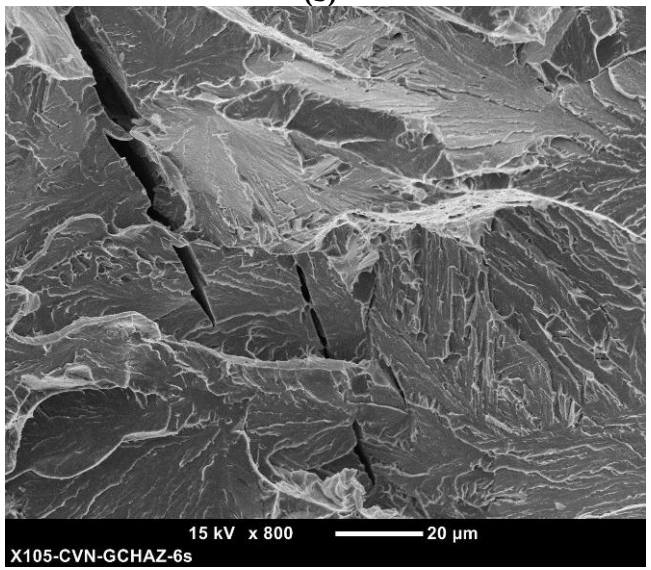

(d)

Figure 22. Fractographs showing detail of fracture surface of X100-5 CVN-GCHAZ $\Delta t_{800\text{-}500}$ = 6 s specimen, 7 J at –80°C.

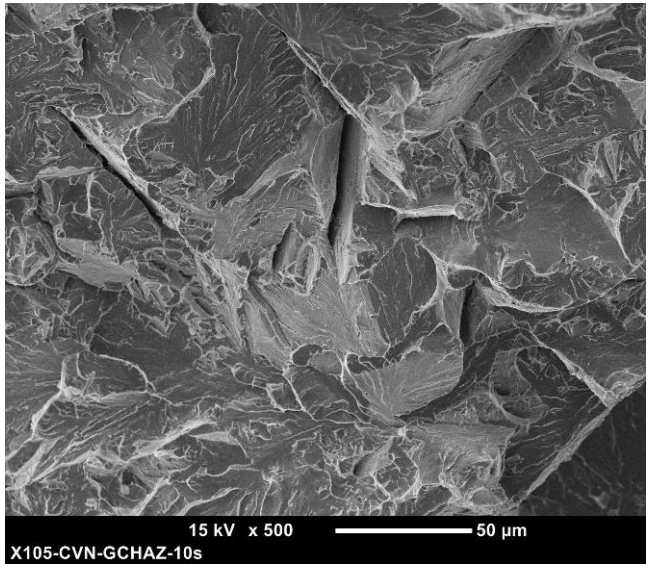

(a)

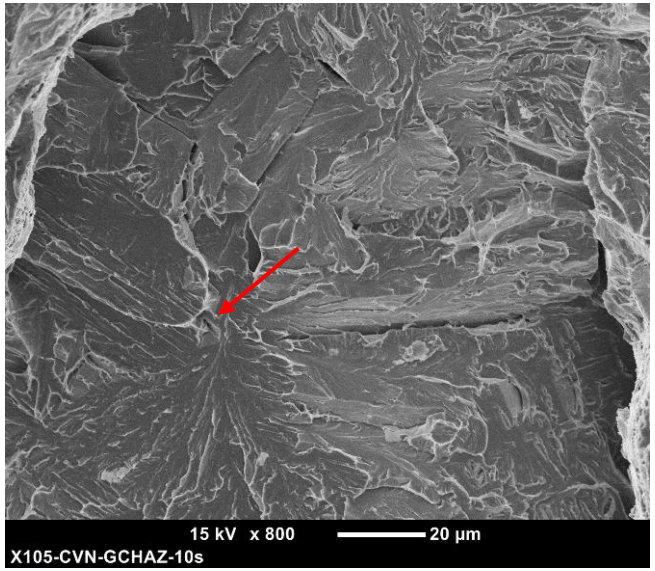

(b)

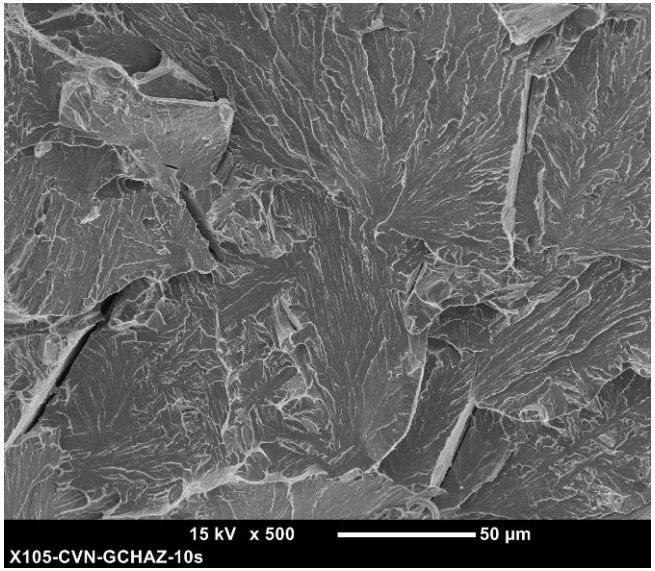

(c)

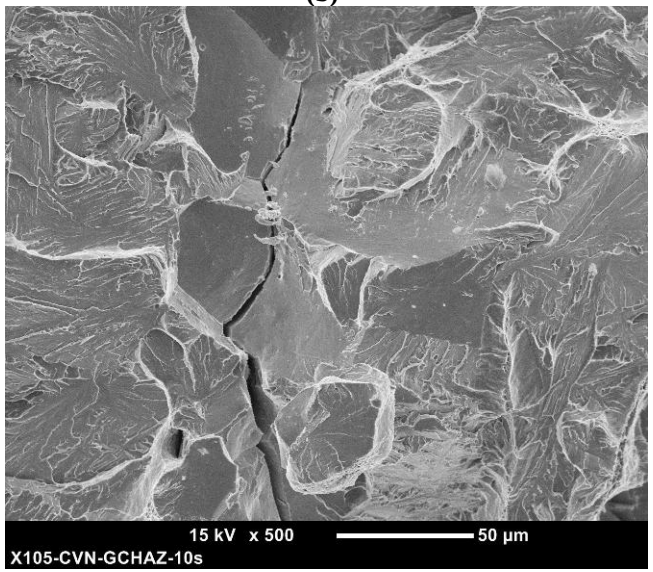

(d)

Figure 23. Fractographs showing detail of fracture surface of X100-5 CVN-GCHAZ $\Delta t_{800\text{-}500}$ = 10 s specimen, 13 J at –60°C.

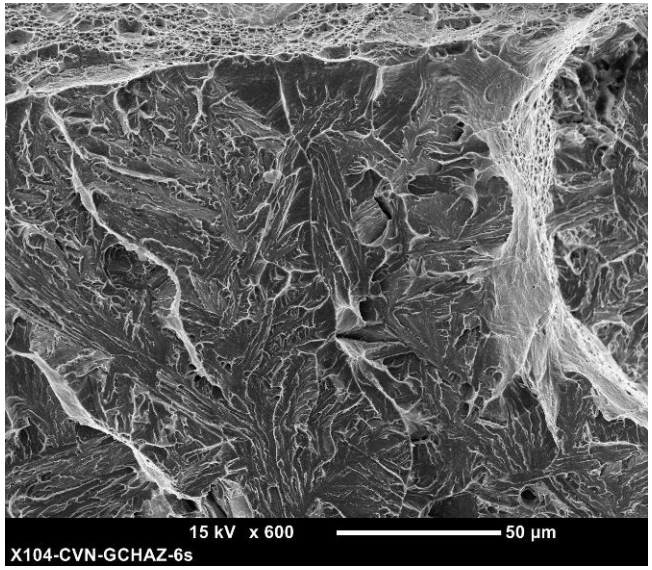

(a)

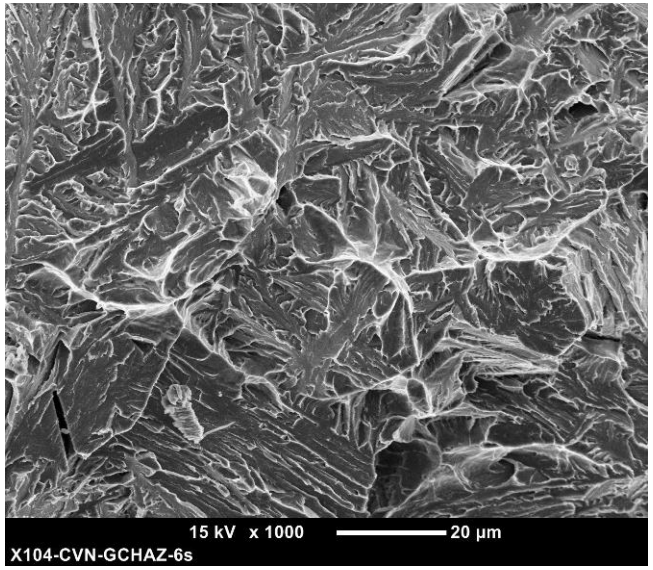

(b)

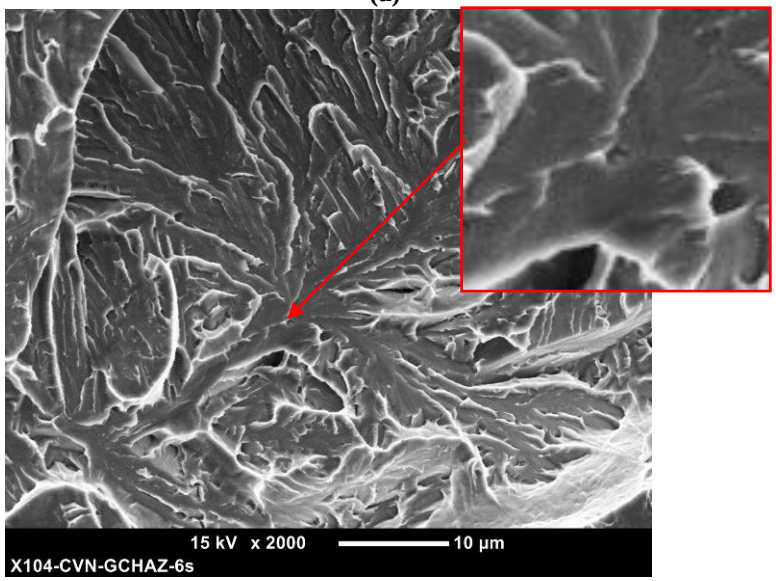

(c)

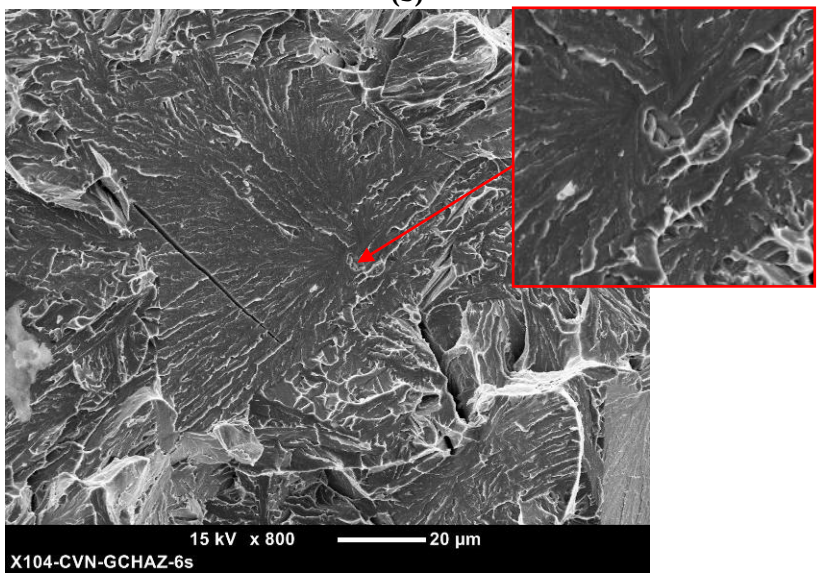

(d)

Figure 24. Fractographs showing detail of fracture surface of X100-4 CVN-GCHAZ $\Delta t_{800\text{-}500}$ = 6 s specimen, 20 J at –80°C.

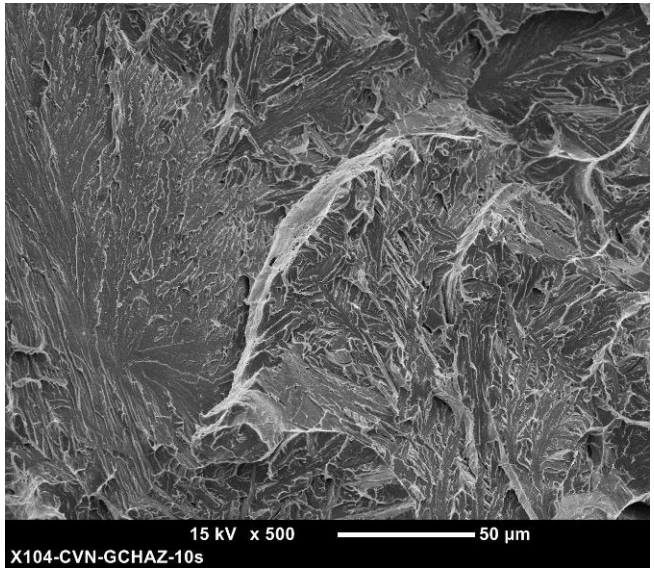

(a)

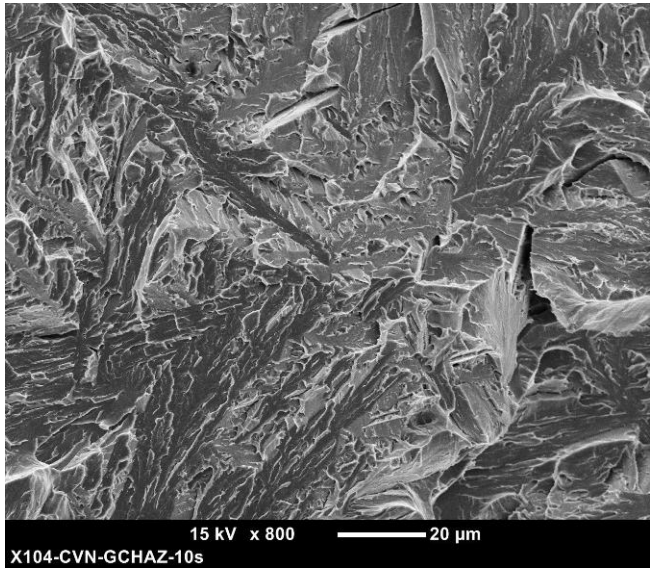

(b)

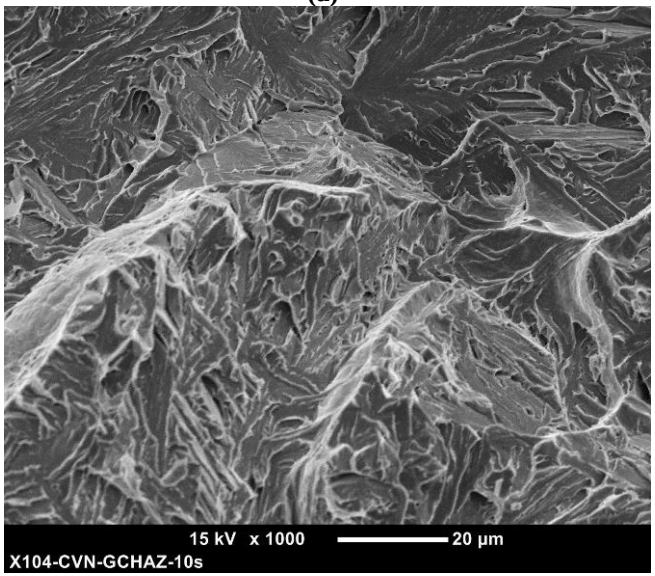

(c)

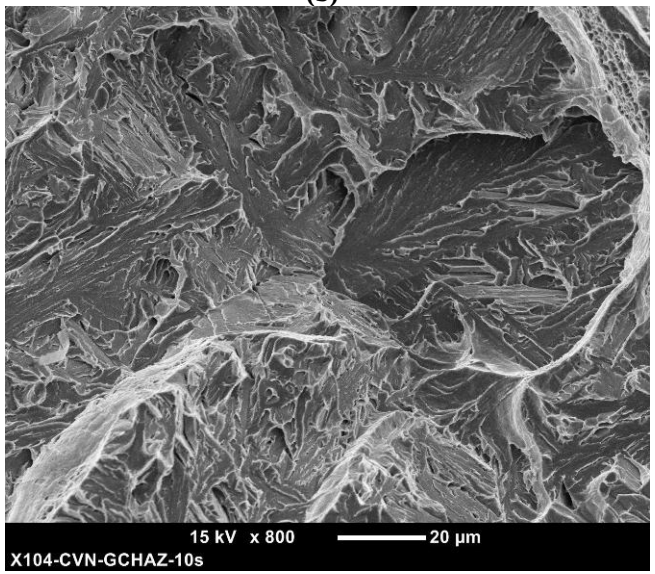

(d)

Figure 25. Fractographs showing detail of fracture surface of X100-4 CVN-GCHAZ $\Delta t_{800\text{-}500}$ = 10 s specimen, 14 J at –80°C.

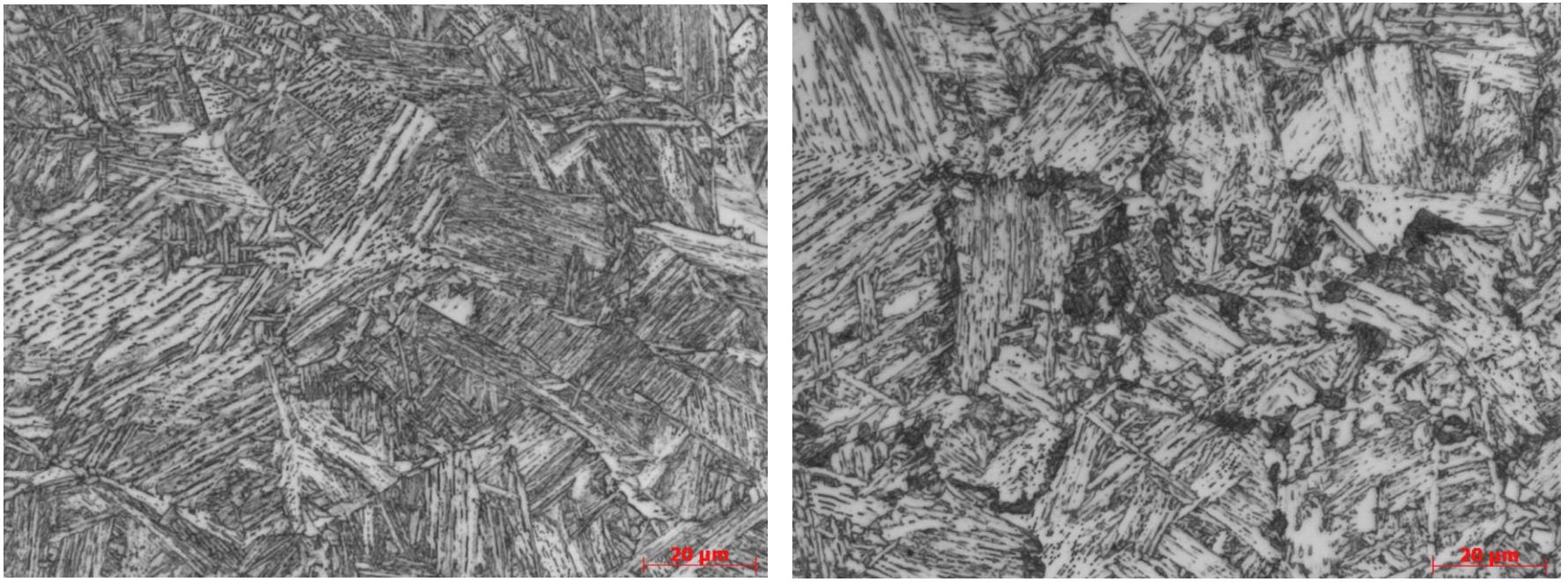

(a) GCHAZ **(b) ICR-GCHAZ**

Figure 26. Micrographs of real weld single torch (a) GCHAZ and (b) ICR-GCHAZ regions in equivalent to X100-5 pipe steel.